

# Geodynamics of Europa's Icy Shell

**Francis Nimmo**

*University of California Santa Cruz*

**Michael Manga**

*University of California Berkeley*

---

Processes that operate within Europa's floating icy shell and leave their signature on the surface are largely governed by the thermal and mechanical properties of the shell. We review how geodynamic models for icy shell dynamics can be integrated with observations to constrain the present and past properties of the icy shell. The near-surface exhibits brittle or elastic behavior, while deeper within the shell viscous processes, including tidal heating, lateral flow, and possibly convection, dominate. Given the large amplitude of topography on Europa, the icy shell is probably more than several kilometers thick at present. However, there are both theoretical models and observational evidence suggesting that the icy shell has been thickening over time, explaining the predominance of extensional features and the young (probably ~50 m.y.) surface age. Geophysical measurements on future missions will be able to determine the present thickness of the icy shell, and possibly its thermal structure.

## 1. INTRODUCTION

Europa's icy shell records a complex tectonic history that reflects an interaction between surface processes, internal structure, and orbital dynamics. The icy shell also separates the hostile surface environment from an inferred subsurface ocean. The nature and history of this shell is thus of great astrobiological, geological, and geophysical importance. In this chapter we will discuss the geodynamics of Europa's icy shell, i.e., its mechanical and chemical properties and evolution, and the processes that are likely to be operating today.

The most direct evidence for an icy shell at present, i.e., a layer of ice separated from a rocky interior by a liquid ocean, is the induced magnetic field produced in a highly electrically conductive (ocean) near-surface region (*Kivelson et al.*, 2000). In addition, models for most of the surface features we see on Europa's surface, including the pits, domes, chaos, bands, and ridges shown in Fig. 1, probably either require the presence of an ocean or involve this water reaching the surface. While the existence of an ocean is generally accepted (see, e.g., chapter by McKinnon et al.), many of the properties and processes in the icy shell remain the subject of considerable uncertainty and debate. Indeed, the Galileo mission, which through its higher imaging resolution identified surface features unseen by the earlier Voyager spacecraft, raised more questions than it answered. Nevertheless, a combination of surface observations and theoretical models allows certain questions to be answered and hypotheses to be tested.

There are two overarching questions on which we focus: (1) What are the origins of the observed surface features? (2) What do the characteristics of surface features tell us about the properties and evolution of the icy shell?

In order to answer these questions, the first two parts of this chapter will consist of theoretical explorations of the likely structure of a floating icy shell, and the different mechanisms available to deform the shell and leave a tectonic record on the surface. Section 4 will then compare these theoretical predictions with observations of Europa's surface to infer the present-day characteristics of the icy shell. Section 5 will carry out a similar exercise focusing on the evolution of the icy shell through time. Section 6 will conclude with a review and suggestions for future work.

Some of the topics we cover in this chapter are discussed in more detail elsewhere in this volume. In particular, Europa's tidal heating, interior structure, thermal evolution and potential icy shell convection are addressed by Sotin et al., Schubert et al., Moore and Hussmann, and Barr and Showman, respectively. Similarly, the global stratigraphy, tectonics, and origin of various landforms are discussed by Doggett et al., Kattenhorn and Hurford, Prockter and Patterson, and Collins and Nimmo. Briefer summaries of the interior and surface geology of Europa may be found in *Schubert et al.* (2004) and *Greeley et al.* (2004), respectively.

Although Europa is primarily composed of silicates and iron (chapter by Schubert et al.), its surface appearance is controlled by the characteristics of the icy shell. Before embarking on a detailed exploration of icy shell geodynamics, it is helpful to consider similarities and differences to the more familiar behavior of the crusts and mantles of silicate bodies.

Ice in terrestrial settings (e.g., glaciers), and even on Mars, is always close to its melting temperature and generally deforms in a ductile fashion. At the ~100-K temperatures relevant to Europa's surface, however, ice is strong and brittle and behaves very much like rock at the surface of the Earth. Thus, common tectonic features on Earth ap-

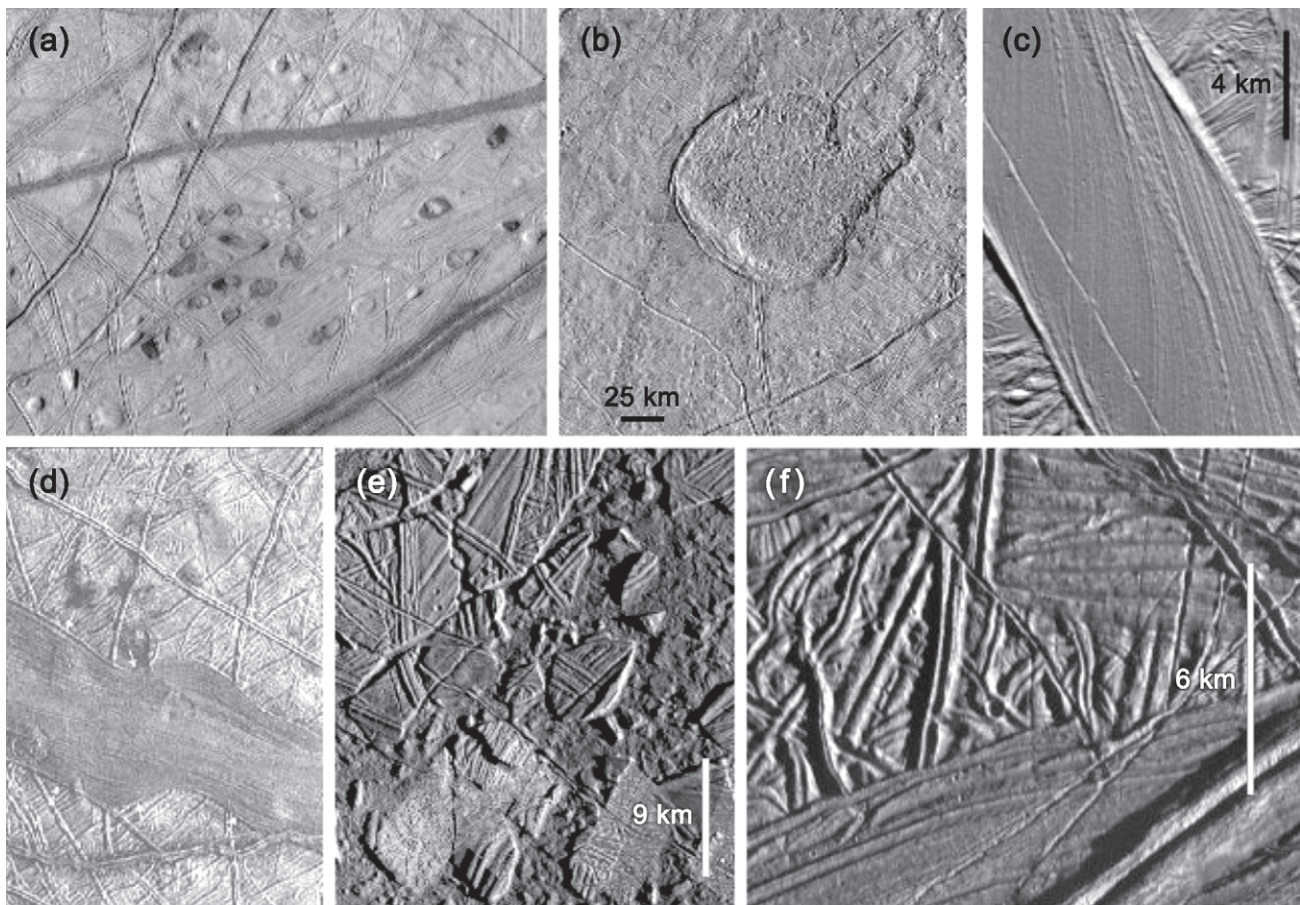


**Fig. 1.** Examples of surface features whose properties are governed by processes within the icy shell: (a) spots, pits and ridges (PIA03878); each pit is about 10 km across; (b) the “Mitten” feature (Murias Chaos) (PIA01640); (c) gray band that records 60 km of strike-slip motion (PIA01643); (d) band showing dilatation (from Prockter *et al.*, 2002); band is about 30 km wide; (e) Conamara Chaos showing blocks that have been displaced and rotated within a low-viscosity substrate (PIA01403); (f) ridges and fractures (PIA00849).

pear to have european analogs (see chapter by Kattenhorn and Hurford), including normal faults (Nimmo and Schenk, 2006), tail cracks (Kattenhorn, 2005), wing cracks (Schulson, 2002), anti-cracks (Kattenhorn and Marshall, 2006), folds (Prockter and Pappalardo, 2000), and strike-slip faults (Hoppa *et al.*, 1999c). An important difference, however, is that ice near its solidus temperature is roughly  $10^6$  times less viscous than rock near its solidus temperature; thus, ductile flow processes (e.g., convection) within Europa’s icy shell happen on much more rapid timescales than similar processes within Earth’s crust and mantle even though typical (tidal) stresses on Europa are much smaller than tectonic stresses on Earth (see section 3).

Perhaps the most fundamental difference is that ice, unlike the lithospheric mantle on silicate bodies, is less dense than the underlying material. Here and elsewhere we are referring to ice I — higher-pressure phases of ice are probably not relevant to Europa’s shell (see chapter by Schubert *et al.*), although they are relevant on other large icy satellites, e.g., Ganymede. One immediate consequence of this effect is that melt (i.e., water) generated by heating of ice will generally drain downward and not upward, with im-

portant consequences for the likelihood of low-temperature (cryo-) volcanism (section 4.2.4). Another is that the (buoyant) floating icy shell will insulate the underlying ocean, potentially allowing it to persist for geological timescales.

The low density of ice I means that subduction of the icy shell into the underlying ocean is not favored, similar to the resistance of continental material to subduction on Earth. Although some features resembling those at divergent terrestrial plate boundaries are observed on Europa (e.g., Sullivan *et al.*, 1998; Prockter *et al.*, 2002), no evidence has been found for features directly resembling subduction zones.

Although subduction is unlikely to generate significant stresses on Europa, tidal stresses, arising from the varying distance and orientation of Jupiter relative to Europa, are much more important than the Moon’s tidal stresses on Earth (e.g., Greenberg *et al.*, 2002). As discussed below, many of the observed surface features are caused directly or indirectly by tidal stresses. Furthermore, friction associated with tidal deformation is more important than decay of radioactive materials in determining the thermal state of Europa’s icy shell (e.g., Cassen *et al.*, 1979; Squyres *et al.*,

1983; Ross and Schubert, 1987; Ojakangas and Stevenson, 1989a). Thus, unlike the terrestrial planets, the orbital evolution of Europa has a direct effect on its thermal evolution, and vice versa (e.g., Hussmann and Spohn, 2004).

A final difference between Europa and most silicate bodies is that Europa's surface is much less heavily cratered, and therefore younger, than those of its neighboring satellites (see chapter by Bierhaus et al.). Unfortunately, the absolute age of Europa's surface is disputed. The more generally accepted impact flux model, based primarily on observations of extant Jupiter family comets, results in a mean surface age of only a few tens of millions of years (Zahnle et al., 2003), or roughly 1% of the age of the solar system. An alternative (Neukum, 1997), which assumes that the age of Gilgamesh on Ganymede is the same as that of the youngest lunar impact basin (Orientale, 3.8 Ga), and that cratering in the jovian system is dominated by asteroids, results in a surface age of 0.7–2.8 Ga (see Pappalardo et al., 1999). In any event, a significant fraction of Europa's history has no geological record, which makes interpreting its evolution challenging; on the other hand, processes that were only relevant during earliest solar system history (e.g., accretion) cannot have contributed to the sculpting of Europa's surface, and we can thus understand the surface and its evolution in terms of orbital dynamics and internal processes that operate at present.

## 2. ICY SHELL STRUCTURE

The geodynamic behavior of the icy shell is controlled by its mechanical properties and thermal evolution. As a starting point, we thus begin with a largely theoretical review of the mechanical and thermal properties of ice that govern the deformation and heat transfer within a planet-scale icy shell.

### 2.1. Rheology

The observable consequences of tectonic stresses depend mainly on the response of the material being stressed, i.e., its rheology. Here we discuss the three main ways in which ice may respond to imposed stresses, and the consequences of these different response mechanisms. At low stresses and strains, ice will deform in an elastic (recoverable) manner. However, at strains greater than roughly  $10^{-3}$ , the ice will undergo irrecoverable deformation. At low temperatures, this deformation will be accomplished by brittle failure, while at higher temperatures the result will be ductile creep.

**2.1.1. Brittle deformation.** Silicate materials typically undergo brittle failure along preexisting faults when the shear stresses exceed some fraction, typically 0.6, of the normal stresses. This behavior is largely independent of composition and is known as Byerlee's rule. At low sliding velocities and stresses, ice obeys Byerlee's law with a coefficient of friction of 0.55 (Beeman et al., 1988), which is independent of temperature, although at higher sliding velocities the behavior becomes more complex (Rist, 1997).

At shallow depths where normal stresses are small and temperatures are low, brittle deformation is expected to dominate on icy satellites.

**2.1.2. Ductile deformation.** At sufficiently high temperatures, ice responds to applied stresses by deforming in a ductile fashion. The response is complicated by the fact that individual ice crystals can deform in several different ways: by diffusion of defects within grain interiors, by sliding of grain boundaries, and by creep of dislocations (Durham and Stern, 2001; Goldsby and Kohlstedt, 2001). Which mechanism dominates depends on the specific stress and temperature conditions, but each individual mechanism can be described by an equation of the form

$$\dot{\epsilon} = A\sigma^n d^{-p} \exp\left(-\frac{Q + PV}{RT}\right)$$

Here  $\dot{\epsilon}$  is the resulting strain rate;  $\sigma$  is the differential applied stress;  $A$ ,  $n$ , and  $p$  are rheological constants;  $d$  is the grain size;  $Q$  and  $V$  are the activation energy and volume, respectively;  $R$  is the gas constant; and  $P$  and  $T$  are pressure and temperature, respectively. In general, for icy satellites the  $P,V$  contribution is small enough to be ignored, and strain rates should increase with increasing temperature and stress and decreasing grain size. When several different mechanisms are operating together, the total strain rate is a superposition (in series and/or parallel) of the individual strain rates (see equation (3) in Goldsby and Kohlstedt, 2001).

At low stresses, diffusion creep is expected to dominate and is predicted to result in Newtonian flow (i.e.,  $n = 1$ ) with a grain-size dependence ( $p = 2$ ). At higher stresses, the dominant creep regimes are basal slip and grain boundary sliding, which result in non-Newtonian behavior ( $n \sim 2$ ) and grain-size dependence. At even higher stresses, strongly non-Newtonian dislocation creep ( $n = 4$ ) dominates. Creep rates are enhanced within about 20 K of the melting temperature (Goldsby and Kohlstedt, 2001), presumably because of the presence of thin films of water along grain boundaries (e.g., De La Chapelle et al., 1999).

Because stresses and strain rates on icy satellites are expected to be low, the most relevant deformation mechanism is probably diffusion creep (e.g., Moore, 2006; McKinnon, 2006), but superplastic flow or dislocation creep may dominate in regions undergoing active convection (Freeman et al., 2006). Diffusion creep has the modeling advantage of resulting in Newtonian behavior, but the disadvantage that the viscosity ( $\eta = \sigma/\dot{\epsilon}$ ) is dependent on the (unknown) grain size, and that the relevant rheological parameters have not yet been measured (Goldsby and Kohlstedt, 2001). Ice grain size evolution is poorly understood, because it depends both on the presence of secondary (pinning) phases and because of dynamic recrystallization processes (e.g., Barr and McKinnon, 2007). Given the uncertainties, it is often acceptable to assume for modeling purposes that ice has a Newtonian viscosity near its melting temperature in the range  $10^{13}$ – $10^{15}$  Pa s (e.g., Pappalardo et al., 1998).

Although the unknown grain size is the most serious unknown for describing the ductile deformation of ice, other effects can also be important. The presence of even small amounts of fluid significantly enhances creep rates (e.g., *De La Chapelle et al.*, 1999). On the other hand, the presence of rigid impurities (e.g., silicates) and salts serves to increase the viscosity (*Friedson and Stevenson*, 1983; *Durham et al.*, 2005a). Finally, higher-pressure phases of ice, or ices incorporating other chemical species such as methane, tend to have much higher viscosities than pure ice at the same P/T conditions (*Durham et al.*, 1998), although ammonia is an exception to this general rule (*Durham et al.*, 1993).

**2.1.3. Elastic deformation.** At low stresses and strains, ice will deform elastically and the relationship between stress  $\sigma$  and strain  $\epsilon$  depends on the Young's modulus  $E$  of the material and is given by Hooke's law:  $\sigma = E\epsilon$ .

Although measurement of Young's modulus in small laboratory specimens is straightforward and yields a value of about 9 GPa (*Gammon et al.*, 1983), the effective Young's modulus of large bodies of deformed ice is less obvious (*Nimmo*, 2004c). Observations of ice shelf response to tidal stresses on Earth (*Vaughan*, 1995) give an effective  $E$  of  $\sim 0.9$  GPa, an order of magnitude smaller than the laboratory values. This discrepancy is most likely due to the fact that a large fraction of the ice shelf thickness is responding in a brittle or ductile, rather than an elastic, fashion (e.g., *Schmeltz et al.*, 2002). A similar effect may arise on icy satellites, and will be discussed later.

**2.1.4. Viscoelastic behavior.** In reality, materials do not behave as entirely elastic or entirely viscous. Rather, they exhibit elastic-like behavior if the timescale over which deformation occurs is short compared to a characteristic timescale of the material, known as the Maxwell time ( $= \eta/G$ , where  $G$  is the shear modulus) (*Turcotte and Schubert*, 2002). Conversely, if the deformation timescale is long compared to the Maxwell time, the material behaves in a viscous fashion. Such compound materials are termed viscoelastic.

The viscoelastic model is especially important for icy satellites because it provides a convenient description of tidal heating (e.g., *Ross and Schubert*, 1989; *Tobie et al.*, 2005). Tidal heating is maximized when the Maxwell time equals the forcing (orbital) period, and decreases in a linear fashion with forcing frequency for much larger or much smaller values (e.g., *Tobie et al.*, 2003). Hence, the amount of tidal heating depends critically on the local viscosity of the icy shell, which is in turn determined mainly by the temperature (section 2.1.2). The Maxwell time of ice near its melting point is roughly  $10^4$ – $10^5$  s, very close to Europa's orbital period of 3.55 d. Thus, tidal dissipation is expected to be important for warm ice on Europa.

**2.1.5. Application to icy shells.** Temperatures near the surface of icy satellites are sufficiently cold, and overburden pressures sufficiently small, that tectonic stresses are likely to result in brittle deformation. However, at greater depths, temperatures will increase, allowing ductile deformation to dominate. If the principal source of stress is bend-

ing, then near the midplane of the bending shell the stresses may be low enough to allow elastic deformation to occur. Thus, in general one would expect a deformed icy shell to consist of the three regions shown in Fig. 2: a brittle near-surface layer, an elastic "core," and a ductile base (e.g., *Watts*, 2001). The interfaces between these zones occur at depths where the stresses due to two competing mechanisms are equal.

The thickness of the near-surface brittle layer in Fig. 2 depends mainly on the temperature gradient, and to a lesser extent on the degree of curvature (bending). Thus, if the brittle layer thickness can be constrained, e.g., by observations of fault spacings (*Jackson and White*, 1989), then the temperature structure at the time of fault formation can be deduced (e.g., *Golombek and Banerdt*, 1986). Similarly, the stress profile shown in Fig. 2 controls the response of the icy shell as a whole to applied bending stresses. The resulting flexural response can be modeled by assuming that the shell is purely elastic with an effective elastic thickness,  $T_e$ , which can be derived from topographic observations. This

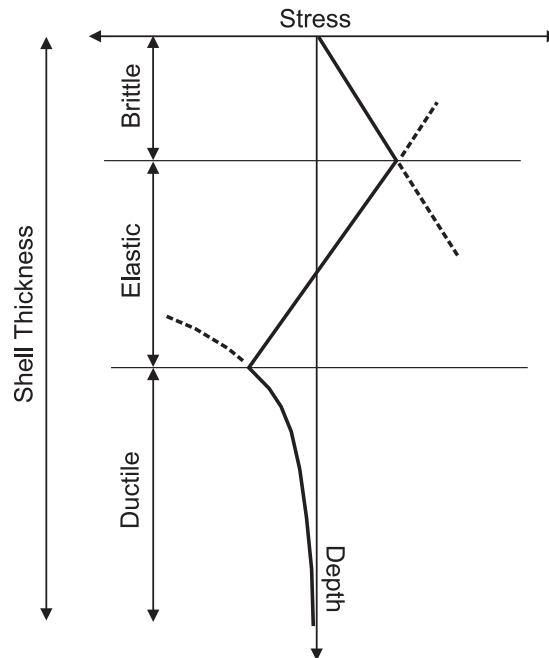


**Fig. 2.** Schematic stress profile within a generic icy satellite shell. Near the surface the ice is cold and brittle and stress increases in proportion to the overburden pressure. Because the shell is undergoing bending, the elastic bending stresses decrease toward the midpoint of the shell and lead to an elastic "core"; the slope of the elastic stress curve depends on the local curvature of the shell and the Young's modulus (e.g., *Turcotte and Schubert*, 2002). At greater depths, the ice is sufficiently warm that the shell deforms in a ductile fashion. The first moment of the stress profile about the midpoint controls the effective elastic thickness  $T_e$  of the icy shell as a whole (e.g., *Watts*, 2001). For typical curvatures seen on Europa,  $T_e$  is controlled mainly by the brittle portion (see section 4.1.1). In equilibrium, the positive and negative areas under the composite stress curve must equal each other (e.g., *Luttrell and Sandwell*, 2006).

effective elastic thickness may be related to the real shell structure (Fig. 2) if the local topographic curvature is known (e.g., Watts, 2001). Hence, estimates of  $T_e$  may be used to determine the thermal structure of icy shells (e.g., Nimmo and Pappalardo, 2004). For an icy shell in which heat transfer occurs only by conduction, knowing the thermal structure in turn allows the shell thickness to be deduced (see section 4.1.1). However, if the icy shell is convecting, then only the heat flux, and not the total shell thickness, can be deduced (section 2.3.2).

## 2.2. Heat Sources

The temperature structure and thickness of the icy shell are determined by the heat being generated, and the rate at which that heat is transported to the surface. There are two principal sources of heat at present: radioactive decay and diurnal tidal dissipation.

Radioactive decay of U, Th, and K is likely confined mainly to silicate minerals and thus occurs within the silicate interior of Europa. Assuming a chondritic composition, the present-day heat production rate results in a surface heat flow of about  $7 \text{ mW m}^{-2}$  (Hussman and Spohn, 2004).

Dissipation due to diurnal tides (see section 3.1) may take place within the silicate interior, within the floating icy shell, or both (dissipation in the ocean is likely small unless the ocean thickness is comparable to the seafloor topography, as on Earth). Dissipation is conventionally modeled as taking place within a viscoelastic body (section 2.1.4) so that the heat generated depends on the viscosity and thus the temperature of the material, as well as the tidal strain rate. Since the temperature in turn depends partly on the heat generation rate, calculation of tidal heating is not straightforward (e.g., Tobie et al., 2005). Furthermore, the presence of a near-surface rigid layer can reduce the overall tidal deformation (Moore and Schubert, 2000), and thus the amount of tidal heating in the interior, although this effect is not pronounced for the relatively thin icy shells expected for Europa.

Tidal dissipation within the icy shell depends on, and influences, the shell temperature structure and thickness and is discussed further below. Because of the spatially variable tidal stress field, tidal dissipation within the icy shell also varies spatially, with the maximum stress and heating occurring at the poles (Ojakangas and Stevenson, 1989a).

Although tidal heating is normally modeled using a viscoelastic approach, other dissipation mechanisms are possible. For instance, laboratory deformation of silicates shows a power-law frequency dependence of dissipation that is not characteristic of Maxwell viscoelastic materials (e.g., Gribb and Cooper, 1998). Perhaps more relevant to Europa is the idea that tidally driven frictional heating on individual faults may also be important in the near-surface (e.g., Gaidos and Nimmo, 2000; Han and Showman, 2008).

Heat, either tidal or radiogenic, generated within the silicate interior is presumed to be transported efficiently across the ocean. The magnitude of the tidal contribution

from the silicate interior is highly uncertain. If this region is cold, tidal dissipation is negligible. If, however, the interior is partially molten (as is thought to be the case for Io), then scaling Io's heat flow to European orbital conditions and assuming similar internal structures results in a heat generation rate of roughly 4 TW (Greenberg et al., 2002) and suggests a thin ( $\approx 4 \text{ km}$ ), conductive shell. Because of the feedback between dissipation and viscosity, tidal heat production in the silicate interior is likely to be either Io-like or negligible, and not some intermediate value (see chapter by Moore and Hussmann). The uncertainty in the amount of tidal heat generated below the ocean is an important contributor to the uncertainty in the icy shell thickness of Europa; uncertainty in the icy shell heat production is another (see below).

## 2.3. Temperature Structure

The temperature structure of the icy shell is one of its most important properties, governing as it does the tendency for different deformation mechanisms to operate (section 2.1) and controlling the flow rate and amount of tidal heating. The detailed temperature structure depends on whether the icy shell is convecting (section 4.2.3) or not. If the shell is not convecting, then the temperature profile will be conductive throughout. If the shell is convecting, then the near-surface ice (the so-called stagnant lid) will be sufficiently cold and rigid that heat is transferred only by conduction, unless some kind of plastic yielding occurs (Showman and Han, 2005). The convective interior, meanwhile, will be approximately isothermal, with a thin boundary layer at its base if significant heat is being transferred from the subsurface ocean. Note that in both the conductive and convective cases the near-surface ice is cold, rigid, and immobile, but that the thickness of the conductive layer relative to the total icy shell thickness is significantly different in these two cases. It is therefore difficult to use inferences of the rigid (elastic) layer thickness to determine the total thickness of the icy shell.

**2.3.1. Conductive portion.** For the conductive portion of an icy shell, it is usually an excellent approximation to assume thermal steady state, in which case the temperature structure depends on the thermal conductivity  $k$ , internal heat sources, and the boundary conditions. The thermal conductivity of ice depends on the temperature  $T$  [a typical approximation is that  $k = 567/T$  where  $T$  is in K and  $k$  has units of  $\text{W m}^{-1} \text{K}^{-1}$  (Klinger, 1980)]. Conductivity can be reduced by near-surface porosity (e.g., Squyres et al., 1983) or the presence of species with significantly lower conductivities, such as methane clathrates (e.g., Nimmo and Giese, 2005). For a conductive icy shell, the bottom boundary temperature is simply the ocean freezing point, which depends on the composition of the ocean (see section 2.4). If the shell is convecting, the base of the conductive lid occurs where the viscosity is roughly an order of magnitude greater than the viscosity in the convective interior of the shell (Davaille and Jaupart, 1994; Solomatov, 1995). For typi-

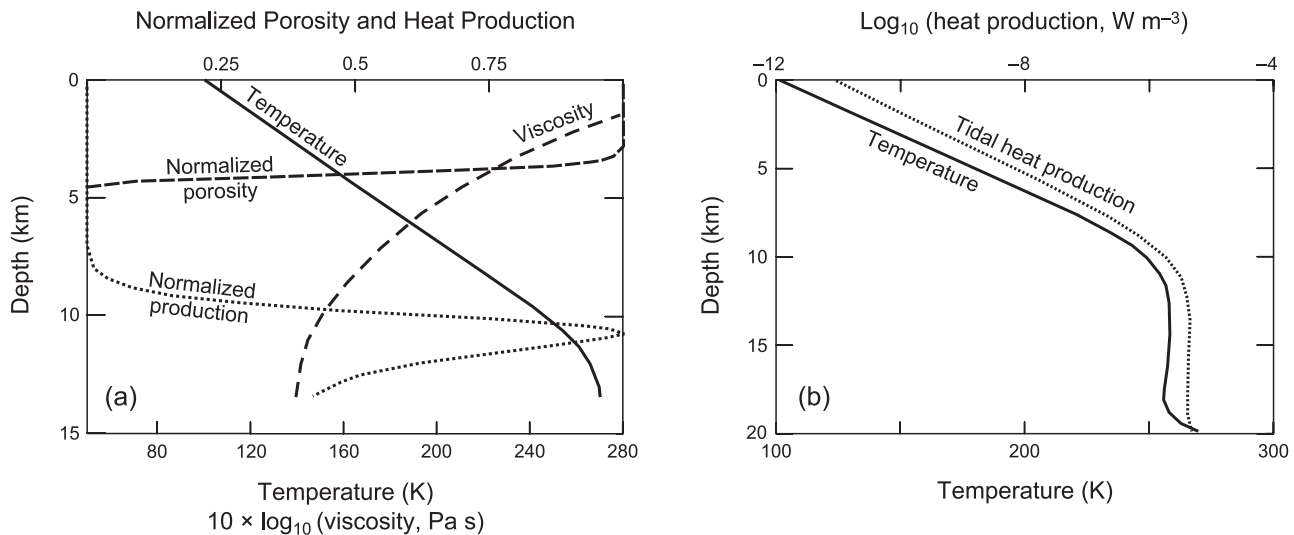


**Fig. 3.** (a) Tidally heated conductive icy shell in thermal equilibrium (steady-state). Temperature, viscosity, and tidal heat production are calculated in a self-consistent manner using the approach of Nimmo *et al.* (2007a). Porosity and heat production are normalized to their maximum values (arbitrary and  $2 \times 10^{-5} \text{ W m}^{-3}$ , respectively). Reference viscosity is  $10^{14} \text{ Pa s}$ , mean strain rate is  $2.1 \times 10^{-10} \text{ s}^{-1}$ , basal heat flux is  $7 \text{ mW m}^{-2}$ , surface heat flux is  $60 \text{ mW m}^{-2}$ , thermal conductivity is  $4 \text{ W m}^{-1} \text{ K}^{-1}$  and equilibrium shell thickness is 13.2 km. This point is located at  $45^\circ\text{N}$ ,  $45^\circ\text{E}$ ; other locations will have different equilibrium shell thicknesses. Porosity evolution is calculated using the method of Nimmo *et al.* (2003a) assuming an evolution timescale of 50 m.y. (b) Tidally heated convective shell in thermal equilibrium, redrawn from Tobie *et al.* (2003). Basal viscosity  $10^{14} \text{ Pa s}$ , ice viscosity ratio  $1.2 \times 10^6$ . Tidal heat production rate was calculated using the temperature profile plotted, but note that the temperature profile was calculated without including the effect of tidal heating.

cal ice activation energies, the corresponding temperature is 230–250 K. In either case the surface temperature varies as a function of latitude, from about 110 K at the equator to ~40 K at the poles (Ojakangas and Stevenson, 1989a). The amount of tidal heating depends on the local temperature; thus, the temperature structure and tidal dissipation profile have to be solved for simultaneously.

Figure 3a shows an example equilibrium temperature profile assuming constant thermal conductivity. The inflection toward the base of the layer is because of tidal heating, which only becomes important at the low viscosities characteristic of ice near its melting point. For a purely conductive icy shell, both the bottom heat flux and the temperature are specified, as is the surface temperature. There thus exists a single shell thickness that can satisfy these constraints simultaneously, in this case 13 km. Hence, in the absence of other effects, the thickness of the conductive icy shell will vary spatially by a few tens of percent, because both the surface temperature and the tidal dissipation vary (Ojakangas and Stevenson, 1989a; Nimmo *et al.*, 2007a). Variations in the thickness of the icy shell can drive horizontal flows that will reduce thickness variations (e.g., O'Brien *et al.*, 2002; Nimmo, 2004a) (section 3.3).

**2.3.2. Convective portion.** The convective interior of an icy shell is close to its melting temperature, which in general results in enhanced tidal dissipation. Figure 3b shows the temperature structure of an example convecting shell and the corresponding heat production. The top half of the shell is cold, highly viscous, and conductive, while the bot-

tom half of the shell is warm, convecting, and approximately isothermal. As with the purely conductive case, tidal heating is greatest in the low-viscosity ice. Note that the temperature gradients in the conductive portions of Figs. 3a and 3b are almost identical, despite the different total shell thicknesses: This example illustrates the difficulty of inferring total shell thickness from shallow temperature gradients alone.

Just as with the conductive case, there is in general, although not always (Mitri and Showman, 2005), only a single shell thickness for which the bottom heat flux and top and bottom temperature conditions can be satisfied in equilibrium (e.g., Moore, 2006; Ruiz *et al.*, 2007). Convective shells generally produce more tidal heating than conductive shells because for the former more of the interior is close to the melting point (Fig. 3). Provided the conductive surface layer remains stagnant because of its high viscosity, the temperature differences within the convecting region will be small,  $\Delta T \sim 2.2 RT_i^2/Q$ , where  $T_i$  is the temperature of the convecting interior (e.g., Solomatov, 1995; Grasset and Parmentier, 1998). For typical ice rheologies,  $\Delta T$  is ~20 K (e.g., Nimmo and Manga, 2002).

An important distinction between conductive and convective icy shells is that for the latter the amount of heat that can be transported across the shell is almost independent of shell thickness (see, e.g., Moore, 2006). Thus, if the basal heating exceeds some critical amount, the only stable solution is a conductive icy shell. For both the convective and the conductive cases, the equilibrium shell thickness

depends mainly on the basal heating (from the silicate interior) and the icy viscosity, neither of which are well known. Thus, the examples shown in Fig. 3 are only representative and whether or not the icy shell is conductive or convective remains uncertain (see section 4.1.3).

## 2.4. Porosity and Contaminants

Modeling studies typically assume that the icy shell is homogeneous pure water ice. In reality, the ice is likely to be heterogeneous in at least two important ways. First, the near-surface is brittle and is continuously being fractured by both impacts and tidal stresses. One would therefore expect the near-surface to contain significant fracture porosity: down to depths of a few meters due to impact processes (see chapter by Moore et al.), and perhaps significantly deeper from tidal fracturing. Of course, at greater depths the ice will lose porosity, either through flow at elevated temperatures [typically 160–180 K; e.g., Nimmo et al. (2003a); Fig. 3] or through brittle compaction (Durham et al., 2005b). However, portions of the near-surface are likely to be porous, with implications for thermal conductivity, vapor transport, surface topography, radar properties, and strength, among other effects. Figure 3a shows a theoretical porosity profile for a conductive icy shell, demonstrating that the top third of the shell, which is cold and relatively rigid, can retain porosity for millions of years.

Second, icy shells are likely to incorporate contaminants, either during rapid freezing or as surficial additions by meteorites or comets. The interplanetary micrometeorite flux at Europa is 45 g/s (Cooper et al., 2001; Johnson et al., 2004) and the mean flux of material ejected from Io by cometary impacts and delivered to Europa is 6–10 g/s (Alvarellos et al., 2008). Over the 50-Ma age of the icy shell, these fluxes imply a mass fraction of <0.0001% assuming a shell 10 km thick and assuming all the delivered materials remain in the icy shell. Spectroscopic studies of the surface of Europa indicate variable fractions of “non-ice” contaminants (e.g., McCord et al., 1998), possibly salts, some of which are preferentially associated with specific geological features such as bands (e.g., Geissler et al., 1998b) and may therefore have been derived from the satellite interior.

Contaminants can have two important effects. First, they will affect the mechanical properties of the icy shell, such as bulk density or viscosity (section 2.1.2). Second, and potentially more important, they can affect the melting behavior of the ice. In particular, the incorporation of salts can dramatically lower the temperature at which the first melts are generated (e.g., Kargel, 1998). Since these first melts are typically salt-rich, a likely way of generating compositional heterogeneity within the icy shell is by partial melting (Nimmo et al., 2003a; Pappalardo and Barr, 2004). Equally, the presence of contaminants such as salts or ammonia in the ocean will reduce its freezing temperature. A colder ocean results in lower temperatures and higher viscosities at the base of the icy shell, and thus lessens the likelihood for icy shell convection. These processes have

several potentially important applications at Europa (sections 3.4 and 4.3.2).

## 2.5. Melting and Cryovolcanism

“Cryovolcanism” refers to the generation and emplacement of low-temperature analogs of silicate volcanic products. These products can involve either “cryomagmas” (low-viscosity water, or higher viscosity water-ice slurry) or vapor. A crucial difference between silicate volcanism and the aqueous cryovolcanism predicted for Europa is that in the latter case the melt (water) is more dense than the solid (ice). Thus, the products of melting are expected to percolate downward, and because of the low viscosity of water, the percolation rate is very rapid (Nimmo and Giese, 2005). Hence one would generally not expect to detect cryovolcanic eruption products at the surface, nor aqueous “cryomagma chambers” at depth. Perhaps not surprisingly, few features on Europa appear to have been generated by cryovolcanic activity (Fagents, 2003) (see section 4.2.4).

Several theoretical mechanisms have been proposed to overcome the density problem. One possibility is that exsolution of dissolved volatiles at shallow depths reduces the volatile-water density to below that of the surrounding ice and drives an eruption (Crawford and Stevenson, 1988). Alternatively, the interaction of silicate magma with ice could lead to overpressures sufficient to drive an eruption (Wilson et al., 1997); note, however, that this mechanism requires the silicates to be in contact with the icy shell, which is implausible given the inferred ~100-km ocean thickness. Showman et al. (2004) suggested that topographically driven flows can force water or a water-ice mixture upward into topographic lows. High pressures within the subsurface ocean can also be generated as the overlying icy shell progressively freezes and thickens (Manga and Wang, 2007; Kimura et al., 2007).

It has been proposed that warm ascending diapirs could cause melting in overlying salt-rich ice (Head and Pappalardo, 1999). However, this model does not overcome the difficulty of downward drainage of melt; furthermore, detailed thermal modeling suggests that the ~100-K surface temperature is very effective in preventing near-surface melting (Nimmo and Giese, 2005), even taking into account the melting-temperature reduction due to salts.

## 3. SOURCES OF STRESS

In this section, we examine mechanisms that could potentially account for the deformation observed at the surface of Europa. Doing so is important partly to develop an understanding of the likely stresses and strain rates characteristic of the icy shell, but also because identifying a particular mechanism (e.g., nonsynchronous rotation) provides clues to both the structure and history of the icy shell. Fortunately, the list of potential mechanisms is considerably simplified by the fact that the surface of Europa is geologically young. This means that mechanisms associated with the early accretion and orbital evolution of satellites (despin-

TABLE 1. Sources and magnitudes of stresses from theoretical work and observations of surface features.

Source	Magnitude	Notes/References	Section
Diurnal tides	<~100 kPa	<i>Greenberg et al. (2002)</i>	3.1
Librations	Comparable to diurnal?	Bills et al. (this volume); <i>Sarid et al. (2006)</i>	4.3.2
Nonsynchronous rotation	Several MPa	<b><i>McEwen (1986); Leith and McKinnon (1996); Geissler et al. (1998a); Sotin et al. (this volume)</i></b>	3.2
Polar wander	Several MPa	<i>Leith and McKinnon (1996); Schenk et al. (2008)</i>	3.2
Thermal convection	<100 kPa	<i>McKinnon (1999); Nimmo and Manga (2002), Tobie et al. (2003); Showman and Han (2004)</i>	3.4, 4.1.3
Compositional convection	<1 MPa	<i>Pappalardo and Barr (2004); Han and Showman (2005)</i>	3.4, 4.1.3
Thickening of the icy shell	Several MPa (tensile)	<i>Nimmo (2004b); Kimura et al. (2007)</i>	3.6
Impacts	TPa	Locally; duration ~ tens of seconds	3.7
Cycloid propagation	<40 kPa	<b><i>Hoppa et al. (1999a)</i></b>	4.3.1
Normal faults	>6–8 MPa	<b><i>Nimmo and Schenk (2006)</i></b>	4.3.3
Band rifting	0.3–2 MPa	<b><i>Stempel et al. (2005); Nimmo (2004d)</i></b>	4.3.3

References in bold denote observationally constrained values.

TABLE 2. Source and magnitude of strain rates.

Source	Magnitude	Notes/References	Section
Diurnal tides	$2 \times 10^{-10} \text{ s}^{-1}$	<i>Ojakangas and Stevenson (1989a)</i>	3.1
Opening of bands	$10^{-15}$ – $10^{-12} \text{ s}^{-1}$	<i>Nimmo (2004d); Stempel et al. (2005)</i>	4.3.3
Nonsynchronous rotation	<~ $10^{-14} \text{ s}^{-1}$	<b><i>Hoppa et al. (1999b)</i></b>	3.2, 4.3.2
Undeformed craters	< $10^{-16} \text{ s}^{-1}$ ?	Assumes <10% local strain and crater age of 30 m.y.; only applies to postcratering deformation	4.3.5

References in bold denote observationally constrained values.

ning, differentiation, core contraction, giant impacts, etc.) are unlikely to be relevant.

Tables 1 and 2 summarize the results of this section, and also include observational constraints on the stress mechanisms and magnitudes (see section 4.3).

### 3.1. Diurnal Tidal Stresses

The single most important source of stress arises from the eccentric nature of Europa's 3.55-d orbit (see chapter by Sotin et al.). Because Europa's orbital period equals its rotation period, Jupiter stays almost fixed in the sky as observed from Europa. However, the orbital eccentricity ( $e = 0.0101$ ) means that Jupiter appears to approach and recede, and also to librate slightly about its mean position in the sky. As a result, the tidal bulge raised by Jupiter (which has a mean amplitude of roughly 1 km) also changes size and position slightly. This time-varying (or diurnal) component of the tide, which scales with the eccentricity, has an amplitude of 30 m if a subsurface ocean is present (e.g., *Moore and Schubert, 2000*) and a period of 3.55 d. It is responsible not only for tidal heating but has also been invoked to explain many of the tectonic features seen at the surface (see below).

Assuming a homogeneous elastic shell, the diurnal tidal stresses and strains are quite low (on the order of 100 kPa and  $10^{-5}$ , respectively) compared with terrestrial near-surface stresses (which are typically tens to hundreds of MPa). However, because of the short orbital periods, the strain rate

( $2 \times 10^{-10} \text{ s}^{-1}$  globally averaged) (*Ojakangas and Stevenson, 1989a*) is much higher than typical terrestrial strain rates. The peak stresses and strains vary with position on the satellite, with the largest values being found at the poles, and minima at the sub- and antijovian points (*Ojakangas and Stevenson, 1989a*).

### 3.2. Other Tidal Effects

As long as the icy shell surface does not shift position relative to the time-averaged (permanent) tidal bulge, only the relatively small diurnal tidal stresses are associated with Europa's orbit. However, if the icy shell shifts relative to the tidal bulge, either due to a change in rotation rate or a reorientation of the surface relative to the rotation axis (i.e., true polar wander, or TPW), then larger stresses arise (e.g., *Matsuyama and Nimmo, 2008*).

Although Europa is observed to be approximately in synchronous rotation, its eccentric orbit means that the tidal torques have the potential to drive it to rotate very slightly faster than synchronous (*Yoder, 1979; Greenberg and Weidenschilling, 1984*). Although these torques can be opposed by torques on mass asymmetries within the icy shell (*Greenberg and Weidenschilling, 1984*), the tendency of ice to flow means that such asymmetries may not persist for geological periods (*Ojakangas and Stevenson, 1989a*). There is thus some theoretical justification for expecting nonsynchronous rotation (NSR) to occur on Europa, and the absence of leading-trailing crater asymmetries on other outer solar sys-

tem satellites (e.g., Ganymede and Callisto) (see Zahnle *et al.*, 2001) suggests that either NSR (or TPW) is a common process, or that the current models of impact fluxes are incorrect.

For Europa, the existence of a subsurface ocean means that the icy shell is decoupled from the solid interior. True polar wander therefore requires a change in the moments of inertia of the icy shell. Large impact basins are one way of achieving this (e.g., Nimmo and Matsuyama, 2007), but such features are not seen on Europa. A more interesting mechanism is that the lateral thickness variations expected for a conductive icy shell (section 2.3.1) may result in a shell that is rotationally unstable (Ojakangas and Stevenson, 1989a,b). In this case, TPW is expected to take place in an approximately continuous fashion and at a rate determined by the thermal diffusion timescale of the icy shell. Observational evidence for NSR and TPW is discussed in section 4.3.2.

Both TPW and NSR involve motion of the permanent tidal bulge with respect to the solid surface, and are therefore described by the same equations (Melosh, 1980). The peak tensional stress is given by (e.g., Leith and McKinnon, 1996)

$$\sigma = 6f\mu \left( \frac{1 + \nu}{5 + \nu} \right) \sin\theta$$

where  $\mu$  is the shear modulus,  $\theta$  is the angle of reorientation,  $\nu$  is Poisson's ratio, and  $f$  is the effective flattening of the satellite. This flattening depends on the geometry of reorientation (Matsuyama and Nimmo, 2008); for instance, flattening is larger along the line joining the pole to the subjovian point than that joining the pole to the center of the leading hemisphere (e.g., Murray and Dermott, 1999). Rather than assuming an instantaneous displacement by an angle  $\theta$ , more recent analyses have compared the reorientation rate with the rate of stress relaxation for a viscoelastic icy shell to determine the stress magnitudes and patterns (Harada and Kurita, 2007; Wahr *et al.*, 2008; chapter by Sotin *et al.*). In either case, the stress patterns generated by NSR or TPW may be calculated and compared with the orientations and styles of geological features.

The stresses generated are large compared with the diurnal tidal stresses, a few MPa compared to roughly 100 kPa, and thus are likely to dominate the tectonic record. However, because the timescales for NSR or TPW are much longer than diurnal timescales,  $>10^4$  yr (Hoppa *et al.*, 1999b), the resulting strain rates are small and the tidal dissipation negligible.

### 3.3. Lateral Shell Thickness Variations

A conductive icy shell may display lateral variations in shell thickness owing to the spatially variable surface temperature and tidal dissipation. Local lateral shell thickness variations may also arise, e.g., due to oceanic plumes of hot water causing local melting of the icy shell (O'Brien *et al.*,

2002; but cf. Goodman *et al.*, 2004). As on Earth, these lateral shell thickness variations result in buoyancy forces that can drive flow from regions where the shell is thick to regions where the shell is thin. The force  $F$  per unit length is given by (e.g., Buck, 1991)

$$F \approx g\Delta\rho t_c \Delta t_c$$

where  $g$  is the acceleration due to gravity;  $t_c$  and  $\Delta t_c$  are the shell thickness and shell thickness contrast, respectively; and  $\Delta\rho$  is the density contrast between icy and water. The stress, if uniform across the entire icy shell, is given by  $g\Delta\rho\Delta t_c$ . For a 1-km shell thickness variation, consistent with expectations from variations in tidal heating (section 2.3.1), the resulting stress is  $\sim 100$  kPa, comparable to the diurnal tidal stresses.

A consequence of these stresses is that the ductile ice near the base of the shell can flow and reduce the shell thickness contrasts. For Newtonian materials the timescale  $\tau$  for this to happen for a feature of wavelength  $\lambda$  is given by

$$\tau \sim \frac{\eta\lambda^2}{g\delta^3\Delta\rho}$$

where  $\delta$  is the thickness of the layer in which flow takes place and is proportional to the shell thickness for conductive shells (Stevenson, 2000; Nimmo, 2004a). The timescale is decreased if the presence of an elastic surface layer is taken into account (Cathles, 1975). Because ice has a low viscosity near its melting point, the flow timescale for local shell thickness variations is geologically short unless the shell is only a few kilometers thick. Figure 4 plots the flow timescale as a function of wavelength and shell thickness and shows that a 100-km wavelength feature will disappear over 50 m.y. unless the shell is thinner than 6 km. Global-scale ( $\sim 4000$  km) shell thickness variations, however, can persist for the same period for shells thinner than roughly 60 km. These results are for conductive shells; if the shell is convecting, relaxation will be geologically instantaneous because of the low viscosity of the warm isothermal interior. Thus, lateral shell thickness contrasts can only be maintained in relatively thin, conductive icy shells.

### 3.4. Density Contrasts and Convection

Lateral variations in density within the icy shell are a possible source of stress. In all cases, the stress  $\sigma$  is given by  $\sigma = dg\Delta\rho$  where  $\Delta\rho$  is the density contrast and  $d$  is the thickness of the anomalous layer.

Thermal and compositional convection are two sources of lateral variations in density. Because the thermal expansivity of ice is relatively low ( $\sim 10^{-4}$  K $^{-1}$ ), the expected 20-K temperature contrast provided by thermal convection alone (section 2.3.2) only results in a density contrast of 2 kg m $^{-3}$  (0.2%). Assuming a typical convective boundary sublayer thickness of 2 km (Nimmo and Manga, 2002) results in maximum stresses of  $\sim 5$  kPa. If the icy shell is salty,

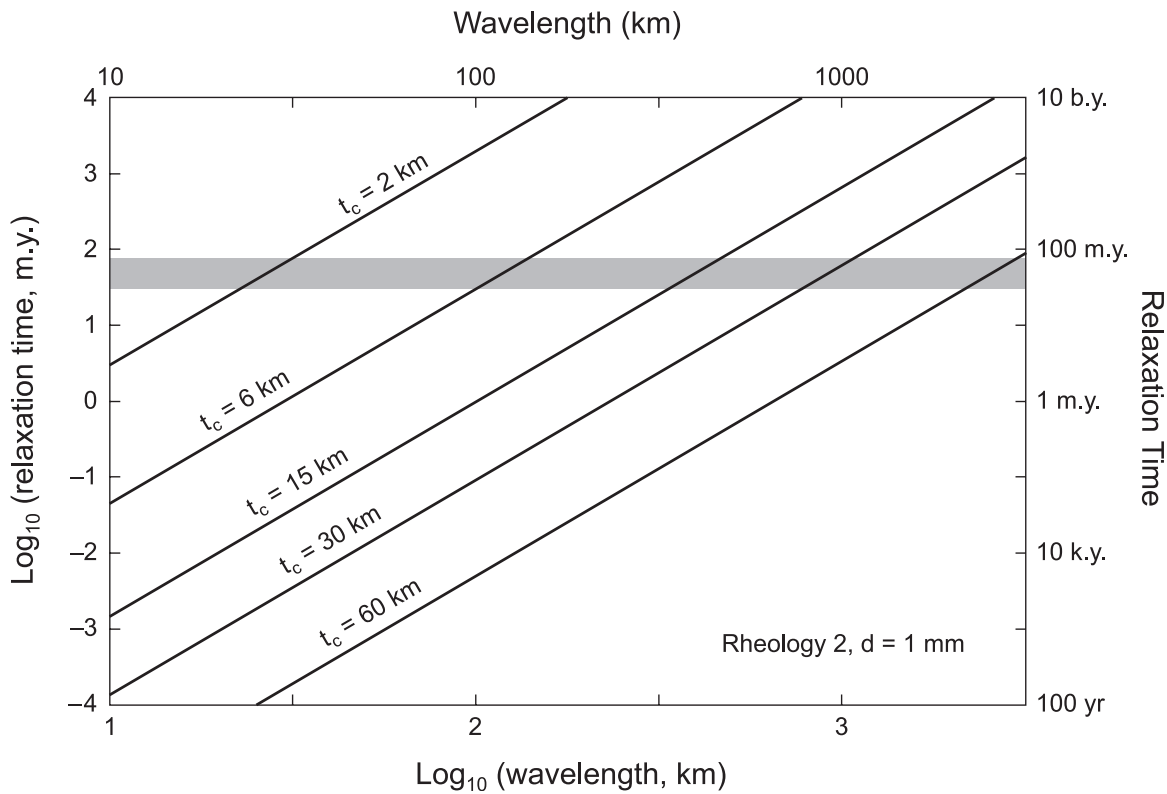


**Fig. 4.** Relaxation timescale as a function of conductive shell thickness  $t_c$  and topographic wavelength. Modified from *Nimmo* (2004a). The shaded band indicates the *Zahnle et al.* (2003) estimated age of Europa's surface;  $d$  indicates ice grain size, and the calculations are carried out for a non-Newtonian ice rheology [GBS-assisted basal slip, in the nomenclature of *Goldsby and Kohlstedt* (2001)].

the coupling between the thermal and compositional convection can lead to larger variations in density. The spatial variations of salinity that would drive such thermochemical convection can arise in several ways: segregation of salt through melting within the convecting part of the icy shell (*Pappalardo and Barr, 2004*); injection of salty water into fractures at the base of the icy shell (*Pappalardo and Barr, 2004*); and incorporation of salts into the base of a thickening icy shell (*Spaun and Head, 2001*). Density differences of a few to as much as 10% might be possible (*Han and Showman, 2005*) and would result in correspondingly larger stresses than those produced by thermal convection alone.

### 3.5. Flexure

If the ice has a finite elastic strength, then the response of the shell to an applied load, whether on the surface or in the subsurface, is distributed over a distance controlled by the elastic thickness  $T_e$  of the shell. The stresses applied by the load are partly or completely balanced by elastic bending stresses within the shell, which depend on the shell thickness and Young's modulus (section 2.1.3) and the local topographic curvature. Thus, observations of apparently flexural features can be used to determine the local elastic thickness and stresses present (see section 4.1.1).

### 3.6. Shell Thickening

Because ice is less dense than water, if the floating icy shell thickens then the surface must move radially outward. Since this outward motion is taking place on a sphere, it is accompanied by global isotropic expansion. This mechanism is an important source of extensional stress for satellites in which the icy shell thickness has increased with time (decreasing thickness leads to corresponding compressional stresses). For thin shells the tangential surface stress  $\sigma_t$  may be derived from *Nimmo* (2004b)

$$\sigma_t \approx \frac{E\Delta t_c \Delta \rho}{(1 - \nu)R\rho_w}$$

where  $\Delta t_c$  is the change in shell thickness,  $\nu$  is Poisson's ratio,  $R$  is the satellite radius, and  $\rho_w$  is the density of water. For Europa, a 1-km change in shell thickness results in a stress of roughly 600 kPa if  $E = 6$  GPa, larger than diurnal tidal stresses. Shell thickening also generates thermal stresses because of the ice cooling, but these are small compared with the volume-change effect (*Nimmo, 2004b; Kimura et al., 2007*). A further consequence of shell thickening is that the pressure in the underlying ocean will increase, with the pressure being determined from a balance between

compression of the ocean water and elastic expansion of the icy shell. *Manga and Wang (2007)* show that while the excess pressure can exceed  $10^4$  Pa, it will not become large enough to allow liquid water to reach the surface. This issue is discussed further in section 4.3.4 below.

### 3.7. Impacts

Because of Europa's young apparent surface age, it is relatively lightly cratered and thus impact craters are less important as a source of stress than on most other icy bodies. The peak stress generated by an impact scales as  $\rho v^2$ , where  $\rho$  is the impactor density and  $v$  the impact velocity (*Melosh, 1989*). Although the peak stresses are thus in the TPa range, they decay rapidly over lengthscales of a few times the impactor radius and timescales on the order of tens of seconds, and are thus only local stress sources.

The topography generated by a crater also gives rise to buoyancy forces (section 3.3), so craters have a tendency to relax over geological time (e.g., *Dombard and McKinnon, 2000*). Such relaxation typically involves surface deformation; however, one of the most puzzling observations is that european craters appear very rarely to be tectonized (*Moore et al., 2001*; chapter by *Bierhaus et al.*) (section 4.3.5).

## 4. OBSERVATIONAL CONSTRAINTS ON ICY SHELL CHARACTERISTICS

Voyager and then Galileo provided images that make it possible to identify processes that may operate within the icy shell and to connect models for these processes to the properties and evolution of the icy shell. We will see that answering some of the fundamental questions remains a challenge: How thick is the ice? Does the icy shell convect? Does cryovolcanism occur? In part the challenge arises because we have access only to images of the surface (and topography in some areas). Gravity, seismological, and heat flow data are not available, in contrast to Earth. A second complication arises because many geodynamic processes are controlled by transitions between solid-like and fluid-like behavior, and cannot distinguish between liquid water and viscous ice. A final complication, discussed in section 5, is that the icy shell thickness is likely changing in time.

### 4.1. Shell Thickness

Perhaps the most important and least-well-known geophysical characteristic of Europa's icy shell is its thickness (*Pappalardo et al., 1999*). The thickness is important because it controls the degree of exchange between the surface and the ocean, which in turn will affect the ocean's astrobiological potential (*Chyba and Phillips, 2002*) and the probability of detecting any astrobiological activity (*Figueredo et al., 2003*). The design of future instruments, especially radar (*Chyba et al., 1998*; *Moore, 2000*), intended to penetrate the ice layer will be significantly affected by the assumed shell thickness. Measuring the shell thickness

is also important because it provides clues to Europa's thermal evolution and current state (see section 5). In particular, estimating the shell thickness places strong constraints on the shell's temperature structure and vice versa (section 2.3). Here, we will describe the different methods used to infer Europa's icy shell thickness; an excellent in-depth review may be found in *Billings and Kattenhorn (2005)*. As will become obvious, there is currently no consensus on the present-day shell thickness; nonetheless, we will try to reconcile the disparate observations.

*4.1.1. Effective elastic thickness.* As discussed in section 2.1.5, the amplitude and wavelength of the icy shell's response to an applied load yields the effective elastic thickness  $T_e$  of the shell (e.g., *Watts, 2001*). The effective elastic thickness is always less than the total icy shell thickness because parts of the shell deform in a brittle or ductile rather than elastic fashion. Nonetheless, thicker shells tend to generate larger values of  $T_e$  and vice versa. Estimating values of  $T_e$  on icy satellites is relatively straightforward; converting  $T_e$  to total shell thicknesses is considerably less so. Another important point to note is that the elastic thickness obtained is the lowest value since the load was emplaced. Thus, if the shell becomes more rigid with time, the deformation in response to a load applied in the past will only place a lower bound on the present-day elastic thickness. Equally, if the shell has undergone viscoelastic relaxation since the load was emplaced (e.g., *Dombard and McKinnon, 2006*), then the estimated value of  $T_e$  may differ from that at the time of loading.

Elastic thickness estimates are most often derived using topographic data. On terrestrial planets topography is typically obtained using altimetric radar or lidar. The Galileo spacecraft did not possess such an instrument, and so topography is derived from images using either stereo or photoclinometric (shape-from-shading) techniques. The former technique is less prone to error, except at the longest wavelengths, but is limited because it requires two images of the same region with suitable viewing geometries and resolutions (e.g., *Giese et al., 1998*). The latter technique has to account for the fact that both slopes and intrinsic albedo contrasts can lead to differences in brightness, and is thus subject to more uncertainties (*Jankowski and Squyres, 1991*; *Kirk et al., 2003*), but it has an intrinsically higher spatial resolution than the stereo technique.

Various approaches to obtaining  $T_e$  values on Europa have been tried, but they all essentially rely on measuring the characteristic wavelength of the shell's response to an applied load (see chapter by *Kattenhorn and Hurford*). This wavelength is controlled by the flexural parameter,  $\alpha$ , which may be directly related to the effective elastic thickness  $T_e$  by

$$\alpha = \left( \frac{T_e^3 E}{3g\rho_w(1-\nu^2)} \right)^{1/4}$$

where  $\rho_w$  is the density of the underlying fluid. Note that the uncertainty in the correct value of  $E$  results in a corresponding uncertainty in  $T_e$ : Larger values of  $E$  yield smaller

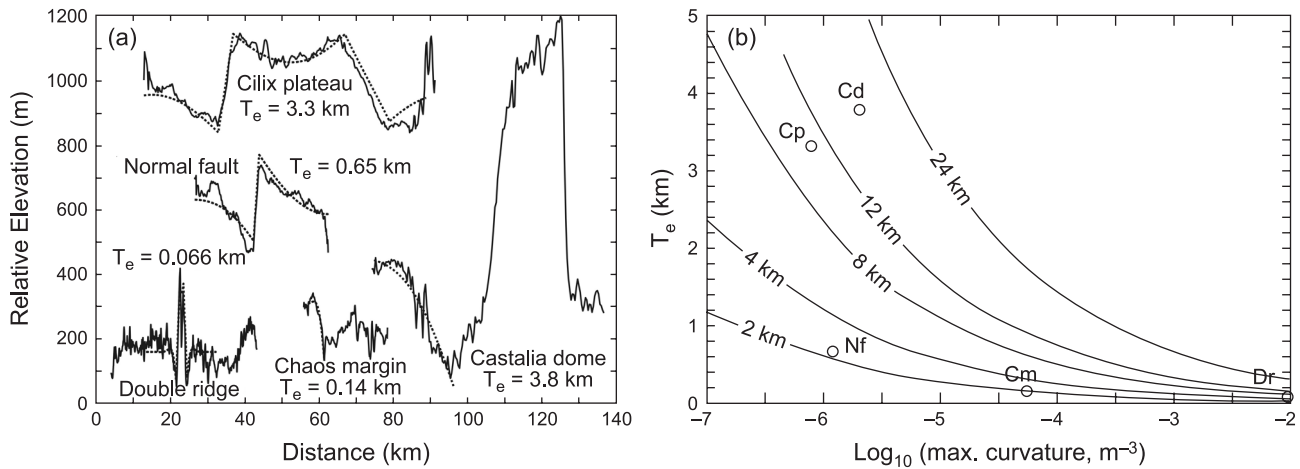


**Fig. 5.** (a) Selected stereo-derived topographic profiles across features on Europa. Solid lines are data; for Cilix, normal fault and chaos margin profiles are averages of multiple individual profiles. Dashed lines are flexural fits, with quoted elastic thickness  $T_e$  and an assumed Young's modulus of 6 GPa. References for original profiles are: Cilix (Nimmo *et al.*, 2003b); normal fault (Nimmo and Schenk, 2006); Castalia dome (Prockter and Schenk, 2005); chaos margin (Nimmo and Giese, 2005); double ridge (Nimmo *et al.*, 2003a). (b) Effective elastic thickness as a function of maximum curvature and conductive shell thickness (contours). Individual points plotted are of the fitted flexural features shown in (a). A strain rate of  $10^{-15} \text{ s}^{-1}$  was assumed, and the method adopted was that of Nimmo and Pappalardo (2004).

$T_e$  values and vice versa. In the figures quoted below,  $T_e$  values will be given using  $E = 6$  GPa throughout.

Flexural responses (Fig. 5a) have been identified at four classes of features on Europa: ridges (Figs. 1a,f), chaos regions (Figs. 1b,e), normal faults, and domes/plateaus (Fig. 1a). Studies of ridges yield elastic thicknesses in the range 0.02–0.66 km (Hurford *et al.*, 2005; Billings and Kattenhorn, 2005). A small-scale updoming near Conamara Chaos yielded a similar range of  $T_e$  (Williams and Greeley, 1998), but larger plateaus near Cilix Crater and at Castalia Macula give values of  $3.3^{+3}_{-1}$  km (Nimmo *et al.*, 2003b) and 3.8 km (Fig. 5a), respectively, for  $E = 6$  GPa. Two normal faults gave values of 0.65 km and 0.08 km, respectively, for  $E = 6$  GPa (Nimmo and Schenk, 2006). Finally, the margins of the Murias Chaos region (Fig. 1b) yielded a value of 4.6 km, with an uncertainty of  $\pm 50\%$  (Figueredo *et al.*, 2002), while the smaller chaos regions imaged in the E15 encounter gave a  $T_e$  of 0.06–0.2 km (Nimmo and Giese, 2005).

The reasons for this order-of-magnitude variability in  $T_e$  estimates are unclear. One possibility is that  $T_e$  varies spatially. For instance, ridges may be areas where shear-heating is important (Gaidos and Nimmo, 2000; Han and Showman, 2008), which could reduce the local rigidity of the ice. On a global scale, variations in the depth to the base of the elastic layer are expected because of spatial variations in tidal heating (section 2.3.1). A second possibility is that  $T_e$  varies in time. For instance, if Europa's icy shell is thickening with time, more ancient episodes of deformation would yield a lower value of  $T_e$ . Although there are not enough impact craters on the surface to allow variations in

surface age to be detected directly, geological observations discussed below (section 5) suggest that a thickening icy shell is possible. A final possibility, which we briefly discuss next, is that the  $T_e$  values are affected by the local topographic curvature. In any case, the large variability in  $T_e$  estimates results in correspondingly large variations in the estimated shell thickness.

One method of converting  $T_e$  estimates to total shell thicknesses is to use the yield-strength envelope approach of McNutt (1984). In this technique, the stress-depth profile is calculated for a variety of shell thicknesses (cf. Fig. 2); the second moment of this profile may be related to the effective elastic thickness of the shell.

Figure 5b plots the predicted effective elastic thickness as a function of topographic curvature and conductive icy shell thickness using the yield-strength envelope technique. As expected, thicker shells result in larger values of  $T_e$ . However, the topographic curvature also has a significant effect: Higher curvatures result in lower values of  $T_e$  for the same shell thickness (because the thickness of the elastic core is reduced — see Fig. 2). This is an important result, because it means that topographic features with different curvatures may produce different  $T_e$  estimates even if the underlying shell thickness is the same. Comparison of these theoretical curves with the individual observations from Fig. 5a suggests a conductive shell thickness in the range 2–18 km.

An important feature of the curves shown in Fig. 5b is that they are quite insensitive to the (poorly known) rheological parameters and strain rate. The reason is that the strength envelope is dominated by the brittle portion of the

icy shell (Nimmo and Pappalardo, 2004). Another feature of these curves is that in the case of convection, the thickness determined is that of the stagnant lid, not the entire shell.

Another approach similar to that outlined above was adopted by Luttrell and Sandwell (2006). These authors used the bending moment implied by European topography to infer the minimum moment associated with the frictional yield-strength envelope (Fig. 2), and thus the minimum thickness of the stagnant part of the icy shell. They obtained a lower bound of 2.5 km, consistent with the range of values derived above. One potential criticism of this work is that the topographic features used were impact craters (Schenk, 2002), which may have been modified by processes such as viscous relaxation (e.g., Dombard and McKinnon, 2000).

**4.1.2. Elevation contrasts and chaos terrain.** Looking for flexural signatures is one way of using topographic information to determine shell thicknesses. Another is simply to focus on elevation contrasts. Topography implies vertical stresses. These could be provided by elastic effects (flexure), but the stresses might also arise from dynamic processes (e.g., convection), or static stresses due to density contrasts (section 3.4). Here we will focus on static stresses, while the next section will focus on dynamic effects.

Assuming zero elastic thickness (i.e., isostatic equilibrium), the topography contrast  $\Delta h$  due to a density contrast  $\Delta \rho$  within a layer of thickness  $d$  is simply  $d\Delta\rho/\rho$ . Since  $d$  cannot exceed the total shell thickness, isostatic elevation contrasts can be used to place bounds on shell thickness. Clearly, it is easier to develop larger topographic contrasts in thick shells rather than thin ones. Furthermore, compositional variations are more likely to result in topographic relief than thermal anomalies because the latter not only generate relatively small density anomalies (section 3.4.1) but are also transient unless a continuous heat source is applied (see Nimmo et al., 2003a).

It is unlikely that  $\Delta\rho$  exceeds the ice-water density contrast, roughly  $100 \text{ kg m}^{-3}$ . Lateral variations in porosity can also generate large density differences, but compaction will limit porosity to the upper quarter to third of the icy shell (e.g., Nimmo et al., 2003a) (see also Fig. 3). A reasonable upper bound for the porosity is 30%, implying maximum depth-averaged density differences of <10%. Since local topographic contrasts on Europa significantly exceed 1 km in some areas (Schenk and Pappalardo, 2004) (Fig. 5a), this implies a lower limit on icy shell thickness of 10 km. Put another way, it is hard to envisage a situation in which the shell thickness is as small as the elevation contrasts observed. This logic, although simple, is perhaps the single strongest argument against thin (few kilometers) icy shells. It is, however, predicated on the assumption of zero elastic thickness, which is not necessarily correct (section 4.1.1). Fortunately, in some cases the issue of  $T_e$  is irrelevant: The 1-km-high dome at Castalia Macula (Fig. 5a) (Prockter and Schenk, 2005) shows a flank trough that implies an elastic thickness of roughly 4 km and a correspondingly larger total shell thickness (about 18 km according to Fig. 5b). Alter-

natively, an isostatically supported dome 1 km high implies a shell thickness of at least 10 km, using the logic above. Thus, at least at the time features with such large relief formed, the conclusion that the shell was thick appears inescapable.

Global shell thickness contrasts (section 2.3.1) will result in isostatically supported topography and are thus susceptible to the same arguments. However, existing Galileo and Voyager limb profile data reveal no evidence for such long-wavelength topography (Nimmo et al., 2007a). This could be due either to the existence of a thin shell (in which case topographic variations exist but are small), or a thick shell in which lateral flow (section 3.3) has erased initial shell thickness variations.

Isostasy arguments have also been applied to chaos regions (Fig. 1e). These disrupted and topographically variable areas were initially interpreted as blocks floating in liquid, on the basis of their morphology (Carr et al., 1998; Williams and Greeley, 1998) and the fact that the blocks have both rotated and translated (Spaun et al., 1998). Block elevation is a few hundred meters; using the same isostatic argument as above yields block thicknesses of 0.2–3 km in Conamara Chaos (Carr et al., 1998; Williams and Greeley, 1998). Unfortunately, it is not clear that the melt-through explanation for chaos formation is unique. More recent examinations of chaos topography (Pappalardo and Barr, 2004; Schenk and Pappalardo, 2004) have invoked diapir-induced deformation. The energy required to generate complete melting of an icy shell would require a concentrated source of heat to be supplied by the underlying ocean, which is dynamically challenging (Collins et al., 2000; Thomson and Delaney, 2001; Goodman et al., 2004). Currently neither the melt-through model nor the competing convective diapirism model for chaos formation (Head and Pappalardo, 1999) appear to be able to explain all the observations (Collins et al., 2000; Nimmo and Giese, 2005). A near-surface low-viscosity substrate is certainly required to allow the chaos blocks to be reoriented and repositioned; however, because of a lack of time information, either ductile ice or liquid water could be the substrate.

**4.1.3. Onset of convection.** One method of inferring the icy shell thickness relies on identifying circular surface features (domes and pits, Fig. 1a) typically ~10 km in diameter as the products of convection within the icy shell. For an icy shell with a fixed temperature difference between top and bottom, the vigor of convection is governed by the Rayleigh number  $Ra$  (see Solomatov, 1995; chapter by Barr and Showman), and convection only occurs for  $Ra > 10^3$ . Thus, if the other parameters in  $Ra$  can be estimated, a lower bound can be placed on the shell thickness for convection to occur (e.g., Pappalardo et al., 1998; McKinnon, 1999; Tobie et al., 2003). The main difficulty is in estimating the effective viscosity of the convecting region  $\eta$ , which for ice is both temperature- and stress-dependent, and also depends on the unknown grain size (section 2.1.2). Most models find that a minimum shell thickness of a few tens of kilometers

is required to initiate convection (e.g., *McKinnon, 1999; Hussmann et al., 2002; Tobie et al., 2003; Moore, 2006*); models incorporating non-Newtonian rheologies tend to require thicker layers (e.g., *Barr et al., 2004*).

A more fundamental issue is whether the domical features observed are really caused by convection, particularly given that they have amplitudes of several hundred meters (*Schenk and Pappalardo, 2004*). The convective stresses responsible for uplift are controlled by the temperature differences within the convecting interior, which are typically only 20 K (section 2.3.1). The resulting stresses do not exceed 0.1 MPa (e.g., *Tobie et al., 2003; Showman and Han, 2004*), which will generate at most 100-m topography. This value is actually an overestimate, because the rigid stagnant lid significantly reduces the observed surface deformation, typically to  $\sim 10$  m (*Nimmo and Manga, 2002*), and warm rising material stalls at the base of this lid, kilometers beneath the surface, unless plastic yielding is invoked (*Showman and Han, 2005*). Furthermore, convection simulations show that topographic lows in response to downwellings have larger amplitudes than the topographic highs (*Showman and Han, 2004*), which does not appear to be the case for domes and pits. Thus, simple convective models currently cannot explain this class of surface features on Europa.

One proposed solution is that tidal dissipation may be concentrated in regions of upwelling, leading to locally larger temperature contrasts, higher stresses, and possibly melting (*Sotin et al., 2002; Tobie et al., 2003*). Another is that thermal convection may be aided by compositional convection (*Pappalardo and Barr, 2004; Han and Showman, 2005*), with the compositional contrasts plausibly arising from partial melting. Reconciling surface observations with sufficiently detailed numerical models of convection is likely to be an active area of research in the future. At present, no convincing alternatives to convection as the source of the domes and pits have been proposed. Equally, though, it is clear that the convection does not take the simple form shown in most models, but probably involves thermochemical, plastic yielding, and/or tidal effects.

**4.1.4. Fracture penetration.** An early argument for the icy shell thickness assumed that extensional features were generated by tidally driven episodic upwelling of the underlying ocean, which required fractures to propagate to the base of the icy shell (*Greenberg et al., 1998*). Similarly, the arcuate nature of cycloids has been explained by appealing to fractures propagating due to diurnal tidal stresses (*Hoppa et al., 1999a*).

It is typically assumed that cracks will propagate to a depth where the overburden pressure is similar to the tensile stress relieved by the crack (e.g., *Gaidos and Nimmo, 2000*). For diurnal tidal stresses of 40 kPa, the implied penetration depth is thus  $\sim 35$  m. Actual tensile cracks will penetrate deeper for two reasons. First, the tensile stress at the crack tip increases as the tensile stress from the fractured region is transferred to the unfractured region. Second, the presence of a traction-free bottom to the icy shell can increase fracture penetration depths compared to the depth

they could penetrate in a half-space (*Lee et al., 2005; Qin et al., 2007*). We caution that all these analyses assume a uniformly stressed icy shell, whereas the lower part of the icy shell, because of its low viscosity, may have much smaller tangential stresses. Because of the low viscosity of ice near the base of the shell, crack initiation (or propagation) there is difficult. However, if such cracks can be initiated, as they propagate upward they will fill with water. The normal stresses on the crack walls are thus reduced, and cracks can much more easily reach the surface (e.g., *Crawford and Stevenson, 1988*). In this case, for tidal stresses of 100 kPa a 2-km-deep fracture could potentially result (*Qin et al., 2007*). In summary, given the current uncertainties in whether liquid water is required to form surface features, and also in the mechanical behavior of the icy shell, the fracture propagation argument does not place a strong constraint on the shell thickness.

**4.1.5. Thermal equilibrium.** In theory, the equilibrium thickness of the icy shell on Europa may be determined by balancing the heat transport through the shell (due to conduction or convection) against the heat produced within the shell (by tidal dissipation) and within the silicate interior (*Ojakangas and Stevenson, 1989a; Hussmann et al., 2002; Spohn and Schubert, 2003; Tobie et al., 2003; Moore, 2006*). Figure 6 shows a typical example of heat production and heat flux as a function of shell thickness. The former increases when convection initiates, because the warm isothermal convecting interior results in a greater volume of ice close to the viscosity at which dissipation is maximized (section 2.1.4). The reduction in heat production for large shell thicknesses is due to the rigidity of the shell reducing the amplitude of the tidal deformation; however, some heat is still generated even when the ocean thickness is zero

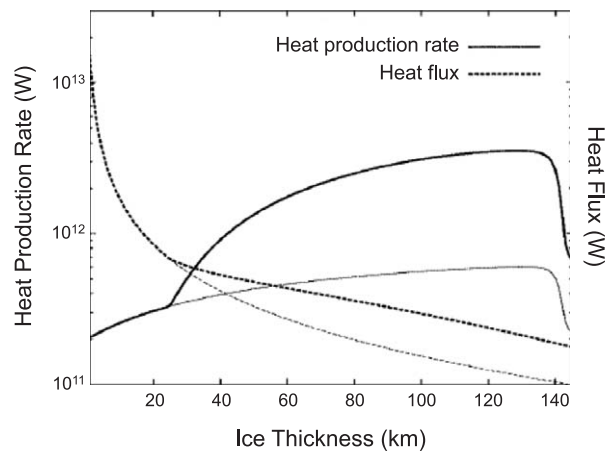


**Fig. 6.** Heat production and surface heat flux as a function of icy shell thickness, from *Hussmann et al. (2002)*. Ice reference viscosity (at 273 K) is  $10^{13}$  Pa s. Convection initiates at 27 km and thermal equilibrium is reached at 35 km shell thickness; initiation of convection may lead to a discontinuous jump in heat flux (*Mitri and Showman, 2005*). Thin lines denote heat flux and production in the (metastable) conductive case. Heat production decreases for thick icy shells because the rigid lid reduces tidal deformation.

(shell thickness 145 km). Heat transport is conductive for shell thicknesses <27 km, and convective thereafter. The convective heat flux decreases with increasing shell thickness because the temperature of the ice at the base of the shell decreases with increasing pressure, leading to an increase in ice viscosity.

Assuming that dissipation within the silicate interior is negligible, equilibrium shell thicknesses are a few tens of kilometers (e.g., *Hussmann et al.*, 2002; *Moore*, 2006) and generally imply convection. However, it is also possible that Europa's mantle resembles that of Io (e.g., *Greenberg and Geissler*, 2002), which is highly dissipative (see section 2.2) and would result in a shell thickness of a few kilometers. Since the state of Europa's silicate mantle is currently unknown (see chapter by *Moore and Hussmann*), models of the kind shown in Fig. 6 are unlikely to resolve the shell thickness debate.

**4.1.6. Impacts.** A final method of estimating shell thickness is to use impacts (see chapter by *Schenk and Turtle*). Large impacts affect deeper regions within the icy shell than smaller impacts; impacts that penetrate the entire shell might be expected to have morphologies distinct from those that do not. A study of crater depth:diameter ratios as a function of crater size yielded two unexpected breaks in slope at diameters  $D = 8$  km and  $D = 30$  km for Europa (*Schenk*, 2002). Although the larger transition diameter was interpreted to imply a shell thickness of 19–25 km, the link between a reduction in depth:diameter ratio and penetration to an underlying ocean has not yet been demonstrated, for instance, by numerical simulations. Numerical simulations that evaluated the preservation of central peaks for euran impact structures placed a lower bound on the shell thickness of 3–4 km (*Turtle and Pierazzo*, 2001), later updated to 5–19 km (*Turtle and Ivanov*, 2002).

**4.1.7. Summary.** Different methods for inferring the icy shell thickness on Europa generate radically different answers. Part of this variability may be due to temporal or spatial variations in shell properties. Elastic thickness determinations differ partly because of the different topographic curvature of different features, but also suggest a shell thickness range of 2–18 km (Fig. 5b). Shell thicknesses as small as 2 km are supported by geological observations of cycloids (because of the limited fracture depths implied by diurnal tidal stresses) and ridges (from  $T_e$  estimates). A shell this thin requires significant tidal heating within Europa's silicate interior. Shell thicknesses of a few tens of kilometers are consistent with observations of impact craters, apparently convective features, and kilometer-scale local elevation contrasts. The latter in particular are a strong argument for a thick shell, which is likely if dissipation in the silicate interior is negligible.

Finally, we note that there are nontectonic constraints on the icy shell thickness. The ocean must be at least a few kilometers thick to explain the magnetometer observations (*Zimmer et al.*, 2000), while *Schilling et al.* (2008) used the same observations to infer an upper bound on the ocean thickness of 100 km. *Hand and Chyba* (2007) obtained an

upper bound on the present-day icy shell thickness of 15 km, although this result depends on the extent to which the apparently strong induction response of the ocean can be separated from other effects such as ionospheric noise.

## 4.2. Icy Shell Structure

Although the thickness of Europa's icy shell is certainly its most important characteristic, various other properties, such as its porosity structure, composition, and lateral variability, may also be constrained by surface observations.

**4.2.1. Porosity and mechanical properties.** Some bands appear to be elevated with respect to their surroundings, suggesting that they contain lower-density material. *Nimmo et al.* (2003a) investigated several potential sources of reduced density, and concluded that bands contain either substantial porosity or cleaner ice relative to the surroundings. Structural features identified as anti-cracks may have formed through reduction of near-surface porosity (*Kattenhorn and Marshall*, 2006). The existence of substantial near-surface porosity is also consistent with Earth-based radar backscatter data (*Black et al.*, 2001).

A consequence of porosity is that both the tensile strength (*Lee et al.*, 2005) and elastic moduli (*Hessinger et al.*, 1996) of ice are reduced. *Lee et al.* (2005) argue that the reduction in ice strength allows cycloidal fracture propagation due to diurnal tidal stresses; *Nimmo and Schenk* (2006) suggest that normal fault displacement:length ratios are characteristic of materials with shear moduli significantly smaller than that of intact ice. Thus, the near-surface of Europa is likely to show strong gradients in porosity and seismic velocity with depth, which is important for future seismic (*Lee et al.*, 2003; *Kovach and Chyba*, 2001; *Panning et al.*, 2006) and electromagnetic (*Chyba et al.*, 1998; *Eluszkiewicz*, 2004) studies. Additionally, a thick, high (tens of percent) porosity layer, if present, implies low thermal conductivity, which results in elevated temperatures in the subsurface and can in some cases result in melting within a few kilometers of the surface (*Nimmo and Giese*, 2005).

**4.2.2. Compositional variations.** Since Europa's surface apparently contains non-ice contaminants (*McCord et al.*, 1998), a natural source of density contrasts is compositional variations. As discussed in section 2.4, many of these contaminants lower the ice melting temperature; thus, warming of contaminated ice will initially produce dense, contaminant-rich melts (e.g., *Head and Pappalardo*, 1999; *Nimmo et al.*, 2003a). Drainage of these melts will produce clean, lower-density ice and lead to potential topographic variations. Thus, localized warming may cause uplift in a contaminant-rich icy shell.

There are several settings where such uplift may be occurring. Domical features and chaos regions have both been suggested as areas where melting-induced compositional contrasts may play a role (sections 4.1.2 and 4.1.3), although at least in the case of chaos regions it proves very difficult to generate the required near-surface melting because of the low surface temperatures (*Nimmo and Giese*, 2005).

Another class of features where compositional variations may be important is bands (Figs. 1c,d). As noted above, several bands appear to be elevated with respect to their surroundings (Prockter *et al.*, 2002). Thermal temperature contrasts are likely to decay on million-year timescales, suggesting that compositional variations are a more likely source of the relief (Nimmo *et al.*, 2003a). If bands are the result of complete (deep) fracturing of a contaminant-rich icy shell and subsequent refreezing of the water (Sullivan *et al.*, 1998), the slowly refreezing ice will not incorporate contaminants and may thus be cleaner than the surrounding material. Alternatively, localized shear-heating (Nimmo and Gaidos, 2002; Han and Showman, 2008) or upwelling of warm ice (Head *et al.*, 1999) could result in partial melting and loss of dense, salt-rich brines, again leading to compositional density contrasts.

**4.2.3. Lateral temperature variations.** There are several reasons why surface or subsurface temperatures might vary laterally. Tidal heating can be localized, for instance, through focused dissipation in a low-viscosity diapir (Sotin *et al.*, 2002) or due to friction along individual faults (Gaidos and Nimmo, 2000). Lateral variations in thermal conductivity or shell thickness would cause lateral temperature contrasts. Extrusion or intrusion of warm material, as may have happened at bands (Prockter *et al.*, 2002) and certain lobate features (Figueredo *et al.*, 2002; Miyamoto *et al.*, 2005), would cause a transient temperature anomaly.

Double ridges (Figs. 1a,f) are features where local temperature anomalies are likely to occur. One possibility is that these ridges form by some combination of linear diapirism (Head *et al.*, 1999) and shear heating (Nimmo and Gaidos, 2002). The latter would result in a transient thermal and topographic anomaly, whereas the former would likely involve flow of ice and permanent uplift. Alternatively, ridges may form by complete cracking of the icy shell and tidal pumping of ice masses to the surface (Greenberg *et al.*, 1998). In this case the thermal anomaly (due to warm water rising to near the surface) would be renewed each tidal cycle. If ridges are indeed the source of local thermal anomalies, this effect may be important in interpreting the local elastic thickness, which may therefore be smaller than the background value (see section 4.1.1). Recent support for the idea of warm ridges has come from Enceladus, where the similar-looking “tiger stripes” are measurably warmer than their surroundings (Spencer *et al.*, 2006), perhaps as a result of shear heating (Nimmo *et al.*, 2007b).

Europa’s surface temperature is controlled by the solar energy input (about  $50 \text{ W m}^{-2}$ ). To cause an observable temperature anomaly, subsurface heat fluxes would have to exceed roughly  $1 \text{ W m}^{-2}$  (Spencer *et al.*, 1999). Flows emplaced at the surface will cool conductively, and at time  $t$  after emplacement the heat flux is roughly  $\rho C_p \Delta T (\kappa/t)^{1/2}$  where  $C_p$  is the specific heat capacity,  $\kappa$  is the thermal diffusivity, and  $\Delta T$  the initial temperature contrast. The thermal anomaly due to a solid-state icy flow will therefore be visible for roughly  $10^3 \text{ s}$  after emplacement, which makes

detection of such an anomaly by a spacecraft very improbable, unless it is being renewed each orbit. More sophisticated models by Abramov and Spencer (2008) result in anomaly lifetimes of a few tens or hundreds of years, still small compared to the likely surface age. On the basis of these arguments, the apparent nighttime thermal anomaly detected by Spencer *et al.* (1999) is more likely due to surface thermal inertia variations than an endogenic heat source.

Finally, lateral surface temperature and tidal heating variations might be expected to lead to global shell thickness and topography variations. However, no such variations have been detected in existing limb profile data (Nimmo *et al.*, 2007a) (section 4.1.2).

**4.2.4. Cryovolcanism.** Despite careful investigation, there is no undisputed evidence for cryovolcanism on Europa. Most candidate features identified from lower-resolution Voyager data were generally revealed as noncryovolcanic when imaged with higher-resolution Galileo instruments (Fagents, 2003). Small, smooth low-albedo regions may be the result of minor flooding (and potentially subsequent drainage) by low-viscosity cryovolcanic liquids (Greeley *et al.*, 2000; Prockter and Schenk, 2005; Miyamoto *et al.*, 2005). Some linear bands have low-albedo margins that may be the result of explosive cryovolcanism (Fagents *et al.*, 2000) (Fig. 1a), although this interpretation is not unique. Some apparently lobate features, including the  $\sim 100\text{-km}$ -wide Murias Chaos region (Fig. 1b), may be the result of extrusive cryovolcanic activity (Figueredo *et al.*, 2002; Miyamoto *et al.*, 2005), although again this interpretation is uncertain.

The lack of unambiguous cryovolcanism on Europa is perhaps not surprising in view of the large density contrast between melt (water) and solid (ice) (section 1). However, the detection of water ice eruption plumes at Enceladus (Porco *et al.*, 2006) serves as a reminder that cryovolcanism can occur, although no such active features were detected at Europa by Galileo (Phillips *et al.*, 2000). Cryovolcanism remains an exciting possibility because it may deliver water from the ocean to the surface.

### 4.3. Sources and Magnitudes of Stress, Strain, and Strain Rates that Create Tectonic Features

By comparing the morphology of surface features with theoretical models for their formation, we can obtain constraints on the stresses and strain rates that formed them. In some cases, this allows us to test different hypotheses for the formation of surface features, identify the dominant sources of stress, or to constrain the thermal and mechanical properties of the icy shell. Tables 1 and 2 summarize sources and magnitudes of stress and strain rates, respectively.

**4.3.1. Diurnal stresses.** At a given location of the surface of Europa, the orientation and magnitude of the diurnal tidal stresses changes over time. If the stresses, possibly in combination with other stresses, exceed the tensile

strength of ice, a crack can form. *Hoppa et al.* (1999a, 2001) proposed that cycloids, arcuate lineaments, form when these stresses exceed the tensile strength of ice so that a crack forms perpendicular to the smallest horizontal stress. The curved shape is a result of the crack propagating through the time-varying stress field. From a calculated stress field, it is possible to predict the trajectory of synthetic cycloids by specifying the stress at which the cycloid starts to form, the stress at which it stops propagating, and the speed at which it propagates. The theoretical results can only match observations by using very low (apparent) crack propagation speeds, typically a few kilometers per hour (e.g., *Hoppa et al.*, 1999a, 2001; *Greenberg et al.*, 2003), rather than the expected speed of crack propagation of  $\sim 1$  km/s (e.g., *Lee et al.*, 2005). Cycloids, if formed in this manner, are thus likely the concatenation of many smaller cracks (*Lee et al.*, 2005). Once a crack is formed, the time evolution of the stress field results in the crack experiencing stresses that may allow for strike-slip motion (*Marshall and Kattenhorn*, 2005) or can initiate new cracks (*Kattenhorn and Marshall*, 2006).

The typical starting and stopping stresses for crack propagation in these simulations are  $\sim 10^4$  Pa, much lower than the tensile strength of intact lab ice, between about 1 and 3 MPa (*Hawkes and Mellor*, 1972; *Schwartz and Weeks*, 1977). One possible explanation for such low stresses causing fracture is that the tensile strength of the European icy shell is low because it is porous or fractured (*Lee et al.*, 2005) (section 4.2.1). Another more likely possibility, discussed below, is that there are additional sources of extensional stress that bring the icy shell closer to failure.

**4.3.2. Other sources of stress needed to explain global fracture patterns.** One common conclusion of models that attempt to reproduce the location and shape of global lineaments is that the icy shell must have experienced some reorientation (*Helpenstein and Parmentier*, 1985; *McEwen*, 1986; *Leith and McKinnon*, 1996; *Geissler et al.*, 1998a). Models for cycloid formation by diurnal tides also favor some reorientation (e.g., *Hoppa et al.*, 2001; *Kattenhorn*, 2002; *Sarid et al.*, 2004; *Hurford et al.*, 2007). A recent study by *Schenk et al.* (2008) demonstrated that the location of 2350-km-diameter, 50-km-wide circular troughs on Europa could be explained by  $\sim 80^\circ$  of polar wander, resulting in stresses of up to 3 MPa.

Nonsynchronous rotation has not been observed directly on Europa, but comparison of Voyager with Galileo images suggests that the NSR timescale must exceed  $10^4$  yr (*Hoppa et al.*, 1999b). The resulting averaged strain rate is thus  $< 10^{-14}$  s $^{-1}$ . In the absence of dissipation, polar wander can occur rapidly ( $\sim 10^3$  yr) (*Ojakangas and Stevenson*, 1989b), leading to correspondingly higher strain rates ( $\sim 10^{-13}$  s $^{-1}$ ).

Polar wander caused by variations in icy shell thickness and nonsynchronous rotation generated by small mean tidal torques can both cause reorientation (section 3.2). Both polar wander and nonsynchronous rotation also generate stresses much larger than the diurnal tides. In fact, the

stresses are comparable to the tensile strength of intact ice and it may thus not be necessary to appeal to additional processes or properties (e.g., porosity) to weaken ice in order to generate tectonic features.

Thickening of a floating icy shell will add an isotropic extensional stress of up to several MPa to the background stress field (*Nimmo*, 2004b) (section 3.6). This effect will thus have no effect on global stress patterns, but will bring features closer to tensile failure.

The tidal dissipation that acts to synchronize Europa's rotation will also reduce its obliquity, but interactions between the Galilean satellites can force Europa to develop a finite (as of yet unmeasured) obliquity (*Bills*, 2005) and undergo librations (*Van Hoolst et al.*, 2008; chapter by *Bills et al.*). *Sarid et al.* (2006) show that a small ( $< 1^\circ$ ) finite obliquity can explain why cycloidal cracks cross Europa's equator and can reproduce their observed shapes. Obliquities of this magnitude generate stresses comparable to those caused by diurnal tides.

**4.3.3. Stresses and strain rates inferred from extensional features.** Extension-related features share many morphological similarities to mid-ocean ridges on Earth (e.g., *Prockter et al.*, 2002) (Figs. 1c,d). Using a mid-ocean-ridge analogy, in which the depth of the brittle-ductile transition is governed by plate cooling, *Stempel et al.* (2005) infer opening rates of 0.3–30 mm/yr and strain rates of  $10^{-14}$ – $10^{-12}$  s $^{-1}$  based on the observed fault spacing. Other rifting models (e.g., *Nimmo*, 2004d; *Manga and Sinton*, 2004) draw roughly similar conclusions but admit the possibility of lower strain rates. The inferred strain rates are much smaller than those from diurnal tides ( $2 \times 10^{-10}$  s $^{-1}$ ; section 3.1), implying that other sources of strain play a key role.

The magnitude of stress inferred from rifting models also provides constraints on the source of stress. *Stempel et al.* (2005) use their value of the tensile strength, 0.5–2 MPa, to infer that nonsynchronous rotation is the driving mechanism for band opening. *Nimmo and Schenk* (2006) compared the topography produced by normal faults with that of flexure models and infer driving stresses that exceed 6–8 MPa. Extensional stresses this large can only be provided by stresses either from cooling icy shells (section 3.6) or possibly NSR/TPW (section 3.2).

**4.3.4. Implications of the paucity of compressive tectonics.** A noteworthy aspect of tectonic features on icy satellites such as Europa is the near absence of features uniquely attributed to compressive stresses. One exception on Europa are small-amplitude folds (*Prockter and Pappalardo*, 2000). The strain accommodated by these folds, however, is much smaller than the strain recorded in bands and they are a minor means to compensate for extension documented elsewhere (*Dombard and McKinnon*, 2006). Cross-cutting relationships across some bands have been interpreted to indicate contraction (*Greenberg*, 2004) and convergence may have occurred both along large, predominantly strike-slip faults (*Sarid et al.*, 2002) and some ridges (*Patterson et al.*, 2006). While bands are typically inter-

preted as being extensional features, *Schulson* (2002) proposed that some wedge-shaped bands are generated by compressive failure.

There are two possible explanations for the small number of compressional features observed on the surface. First, the stress field truly could be truly dominated by extension, which, combined with the lower failure strength of ice under tension than compression, leads to more failure and deformation under extension. Such a situation would occur if, for instance, Europa's shell had been thickening with time (sections 3.6 and 5). However, while the extensional stresses caused by icy shell thickening are large, the global strains are small (few tenths of a percent) (*Nimmo*, 2004b) compared with the estimated global strain across bands of about 5% (*Figueredo and Greeley*, 2004).

Second, compressional tectonic features could be present but difficult to detect. For instance, if each band contained a small compressional component, the global compressional strain accommodated could be significant. The true solution is a probably a combination of these two explanations.

**4.3.5. Impact craters.** If lower bounds on strain rates associated with bands are global, we would expect significant deformation of at least some impact craters. Assuming a mean age of 10 Ma for craters, and a lower bound on strain rates of  $10^{-15} \text{ s}^{-1}$ , mean strains should exceed or be close to 1. No impact craters show strains even close to this value (*Moore et al.*, 2001). This implies that surface deformation is highly localized. Moreover, given the ubiquity of tectonic features on Europa and their comparative rarity within craters, the strength of ice below craters may be higher than that typical of the icy shell. Alternatively, most of the tectonism on Europa may have occurred over a short time period during the earliest history preserved on the present icy shell, so that subsequent impact craters remain relatively undisturbed.

## 5. EVOLUTION OF THE SHELL THROUGH TIME

The manner in which Europa's shell and interior evolved to their present-day states represents a major unsolved problem for at least three reasons. First, the present-day state, especially of the silicate interior, is poorly known. Second, Europa's surface may only record the last 1% of its existence, so there are few constraints on its earlier history. Third, the thermal and orbital evolution of Europa are intimately coupled in a manner that is nontrivial to model (*Hussmann and Spohn*, 2004; see chapter by *Moore and Hussmann*). Nonetheless, both observational and theoretical approaches are starting to yield important insights into Europa's evolution.

Based on observational approaches, there are now several lines of evidence that Europa's shell is not in steady state. First, although the young surface age could be the result of an equilibrium between the creation of impact features and their destruction (presumably through tecton-

ism), the fact that very few craters are tectonically deformed suggests some kind of rapid resurfacing event followed by relative quiescence (*Figueredo and Greeley*, 2004). A similar scenario has been proposed for Venus but with a much longer time interval between resurfacing events (*Strom et al.*, 1994). Second, as noted above, some of the discrepancies in  $T_c$  estimates may be due to temporal variations in shell properties. For example, *Hurford et al.* (2005) find that flexure at younger ridges requires a thicker elastic layer than at older ridges, implying a thickening of the icy shell. Third, regional-scale geological mapping suggests that certain types of features, notably chaos regions, dominate the most recent geologic record preserved on the surface (*Figueredo and Greeley*, 2004; cf. chapter by *Bierhaus et al.*). While this effect may be due to difficulties in identifying ancient chaos terrains (*Riley et al.*, 2000), it suggests that the geological behavior of Europa has changed with time (*Pappalardo et al.*, 1999). Such geological histories may also help distinguish between models for the formation of surface features. For example, if the shell is thickening, and chaos regions are forming more frequently, then models for chaos formation that appeal to diapirism are more plausible than melt-through models as the latter are favored by thin icy shells and the former favored by thick icy shells.

If Europa's icy shell is currently thickening, there may be important tectonic consequences. As the icy shell thickens, near-surface material moves radially outward, and thus experiences extensional stresses (*Nimmo*, 2004b; *Manga and Wang*, 2007; *Kimura et al.*, 2007). The stresses generated are large enough to dominate other likely sources of stress in the icy shell, and their extensional nature may help to explain the dominance of features formed by extensional on Europa (section 4.3.4).

Coupled thermal-orbital evolution models can be used to investigate whether a thickening icy shell is likely, and the timescales over which any thickening occurs, but such models are complicated. The dissipation and transport of heat within the icy shell are highly uncertain because of uncertainties in the ice rheology. More importantly, dissipation in the silicate interior depends sensitively on the viscosity, and thus temperature, of the interior; however, the interior temperature also depends strongly on the amount of dissipation. Modeling this feedback is also complicated by the fact that the evolution of Europa's orbital parameters depend on the behavior of Io and Ganymede (see chapters by *Moore and Hussmann* and *Sotin et al.*). The upshot is that even simplified models show a rich spectrum of behavior (*Ojakangas and Stevenson*, 1986; *Fischer and Spohn*, 1990; *Hussmann and Spohn*, 2004). A particularly interesting result is that Europa's icy shell thickness can show strong oscillations, because of oscillations in Io's behavior (Fig. 7). These arise because of the feedback between dissipation and heat transport in Io's interior, and have a period governed by the ability of Io's mantle to respond to a change in heat production. Although these studies are in their infancy, the importance of these results is that oscillatory behavior is

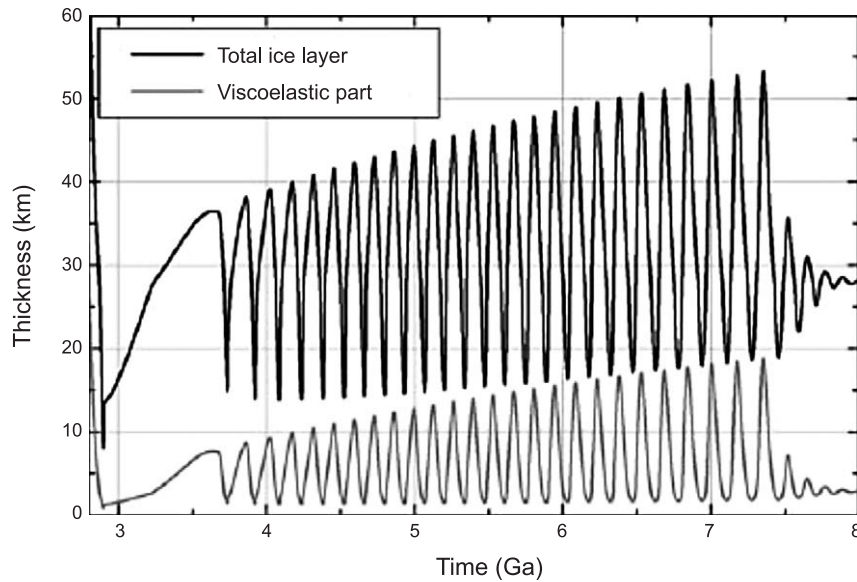


**Fig. 7.** Variation in Europa shell thickness with time, from *Hussmann and Spohn (2004)*. The bold and thin lines refer to the total shell thickness and the viscoelastic part, respectively. The oscillations have a  $\sim 150$  m.y. periodicity and arise primarily because of the coupled thermal-orbital behavior of Io. The model was started with all three bodies in resonance, and 4.5 Ga is the time at the present day.

consistent with the arguments above that Europa's icy shell is not in steady state. As an aside, we note that there are strong arguments that Enceladus, an active saturnian satellite, cannot be in steady state (*Meyer and Wisdom, 2007*). If Europa has undergone oscillatory behavior, this may help to explain why the surface is apparently so young, and also explain why inferences about icy shell thickness and structure based on models for features of different ages are not consistent with each other.

## 6. SUMMARY, OUTSTANDING PROBLEMS, AND FUTURE WORK

The most important property of Europa's icy shell is its thickness because it governs the rheological structure of the icy shell, which in turn controls its tectonics and formation of surface features. The most compelling argument that the shell is thick at present is the large amplitude of topography (Fig. 5). This does not mean that all the features preserved on the surface of Europa are produced by processes that operated in a thick icy shell, as there is both observational evidence for temporal changes in the style of tectonism and theoretical reasons for the icy shell to change thickness (section 5).

If the shell thickness exceeds 10 km, as suggested by the topography, then it is most likely convecting (section 4.1.3). Convection may be responsible for some surface landforms (e.g., spots and domes), but the topography of such features is hard to explain, at least with current thermal convection models.

Whether the icy shell is presently getting thicker or thinner cannot be determined, but we suggest that given the dominance of extensional features and the fact that thickening icy shells generate large extensional stresses, the icy shell is more likely to be getting thicker. The absence of

tectonized craters suggest that this thickening was accompanied by a relatively abrupt change in resurfacing style. The relatively young surface age is consistent with theoretical models of tidally driven oscillatory behavior in which Europa's icy shell thins and then thickens.

Several outstanding questions about the geodynamics and evolution of the icy shell remain, besides determining the present and past thickness of the icy shell: Why is the icy shell so young? Is the icy shell tectonically active today? Does and has liquid water from the ocean reached the surface? Answering these questions may also allow us to determine whether the silicate interior is cold or hot — a feature that in turn will determine whether hydrothermal processes operate within the ocean.

Future missions have the potential of using geophysical techniques to answer some of these questions. Despite the challenging nature of the radiation environment around Europa, radio tracking of an orbiter equipped with a laser or radar altimeter would be able to directly detect diurnal tidal variations and thus conclusively demonstrate the presence or absence of a subsurface ocean, as well as potentially measuring the shell thickness (*Wahr et al., 2006*). Another method of determining the icy shell thickness is by ice-penetrating radar (*Chyba et al., 1998*), although ice absorption (*Moore, 2000*) or near-surface porosity (*Eluszkiewicz, 2004*) might make doing so difficult. Global topography and gravity measurements would allow accurate determination of the icy shell elastic thickness, as has been done, e.g., for Mars (*McGovern et al., 2002*). If the icy shell is currently tectonically active, radar interferometry would be able to detect surface displacements on the order of 10 cm (*Sandwell et al., 2004*). Although landing a surface package is technically challenging, seismological data, even from a single instrument, would allow determination of Europa's internal structure, including the icy shell thickness (*Kovach*

and Chyba, 2001; Lee et al., 2003; Panning et al., 2006). Finally, global multispectral mapping of the kind that Galileo was unable to perform would allow the stratigraphy and history of the icy shell to be resolved with much greater confidence than at present.

**Acknowledgments.** Funding was provided by NASA's Planetary Geology and Geophysics and Outer Planets Research Programs. We thank H. Hussmann, O. Grasset, and D. Sandwell for careful reviews.

## REFERENCES

- Abramov O. and Spencer J. R. (2008) Numerical modeling of endogenic thermal anomalies on Europa. *Icarus*, *195*, 378–385.
- Alvarellos J. L., Zahnle K. J., Dobrovolskis A. R., and Hamill P. (2008) Transfer of mass from Io to Europa and beyond due to cometary impacts. *Icarus*, *194*, 636–646.
- Barr A. C. and McKinnon W. B. (2007) Convection in ice I shells and mantles with self-consistent grain size. *J. Geophys. Res.*, *112*, E02012, DOI: 10.1029/2006JE002781.
- Barr A. C., Pappalardo R. T., and Zhong S. J. (2004) Convective instability in ice I with non-Newtonian rheology: Application to the icy Galilean satellites. *J. Geophys. Res.*, *109*, E12008.
- Beeman M., Durham W. B., and Kirby S. H. (1988) Friction of ice. *J. Geophys. Res.*, *93*, 7625–7633.
- Billings S. E. and Kattenhorn S. A. (2005) The great thickness debate: Ice shell thickness models for Europa and comparisons with estimates based on flexure at ridges. *Icarus*, *177*, 397–412.
- Bills B.G. (2005) Free and forced obliquities of the Galilean satellites of Jupiter. *Icarus*, *175*, 233–247.
- Black G. J., Campbell D. B., and Nicholson P. D. (2001) Icy Galilean satellites: Modeling radar reflectivities as a coherent backscatter effect. *Icarus*, *151*, 167–180.
- Buck W. R. (1991) Modes of continental lithospheric extension. *J. Geophys. Res.*, *96*, 20161–20178.
- Carr M. H. and 21 colleagues (1998) Evidence for a subsurface ocean on Europa. *Nature*, *391*, 363–365.
- Cassen P., Reynolds R. T., and Peale S. J. (1979) Is there liquid water on Europa? *Geophys. Res. Lett.*, *6*, 731–734.
- Cathles L. M. (1975) *The Viscosity of the Earth's Mantle*. Princeton Univ., Princeton.
- Chyba C. F. and Phillips C. B. (2002) Europa as an abode for life. *Origins Life Evol. Biosphere*, *32*, 47–68.
- Chyba C. F., Ostro S. J., and Edwards B. C. (1998) Radar detectability of a subsurface ocean on Europa. *Icarus*, *134*, 292–302.
- Collins G. C., Head J. W., Pappalardo R. T., and Spaun N. A. (2000) Evaluation of models for the formation of chaotic terrain on Europa. *J. Geophys. Res.*, *105*, 1709–1716.
- Cooper J. F., Johnson R. E., Mauk B. H., Garrett H. B., and Gehrels N. (2001) Energetic ion and electron irradiation of the Galilean satellites. *Icarus*, *149*, 133–159.
- Crawford G. D. and Stevenson D. J. (1988) Gas-driven water volcanism and the resurfacing of Europa. *Icarus*, *73*, 66–79.
- Davaille A. and Jaupart C. (1994) Onset of thermal convection in fluids with temperature-dependent viscosity — application to the oceanic mantle. *J. Geophys. Res.*, *99*, 19853–19866.
- De La Chapelle S., Satelnuo O., Lipenkov V., and Duval P. (1999) Dynamic recrystallization and texture development in ice as revealed by the study of deep ice cores in Antarctica and Greenland. *J. Geophys. Res.*, *103*, 5091–5105.
- Dombard A. J. and McKinnon W. B. (2000) Long-term retention of impact crater topography on Ganymede. *Geophys. Res. Lett.*, *27*, 3663–3666.
- Dombard A. J. and McKinnon W. B. (2006) Folding of Europa's icy lithosphere: An analysis of viscous-plastic buckling and subsequent topographic relaxation. *J. Struct. Geol.*, *28*, 2259–2269.
- Durham W. B. and Stern L. A. (2001) Rheological properties of water ice — Applications to satellites of the outer planets. *Annu. Rev. Earth Planet. Sci.*, *29*, 295–330.
- Durham W. B., Kirby S. H., and Stern L. A. (1993) Flow of ices in the ammonia-water system. *J. Geophys. Res.*, *98*, 17667–17682.
- Durham W. B., Kirby S. H., and Stern L. A. (1998) Rheology of planetary ices. In *Solar System Ices* (B. Schmidt et al., eds.), pp. 63–78. Kluwer, Dordrecht.
- Durham W. B., Stern L. A., Kubo T., and Kirby S. H. (2005a) Flow strength of highly hydrated Mg- and Na-sulphate hydrated salts, pure and in mixtures with water ice, with application to Europa. *J. Geophys. Res.*, *110*, E12010.
- Durham W. B., McKinnon W. B., and Stern L. A. (2005b) Cold compaction of water ice. *Geophys. Res. Lett.*, *32*, L18202.
- Eluszkiewicz J. (2004) Dim prospects for radar detection of Europa's ocean. *Icarus*, *170*, 234–236.
- Fagents S. A. (2003) Considerations for effusive cryovolcanism on Europa: The post-Galileo perspective. *J. Geophys. Res.*, *108*, DOI: 10.1029/2003JE002128.
- Fagents S. A., Greeley R., Sullivan R. J., Pappalardo R. T., and Prockter L. M. (2000) Cryomagmatic mechanisms for the formation of Rhadamanthys Linea, triple band margins, and other low-albedo features on Europa. *Icarus*, *144*, 54–88.
- Figueredo P. H. and Greeley R. (2004) Resurfacing history of Europa from pole-to-pole geological mapping. *Icarus*, *167*, 287–313.
- Figueredo P. H., Chuang F. C., Rathbun J., Kirk R. L., and Greeley R. (2002) Geology and origin of Europa's "Mitten" feature (Murias Chaos). *J. Geophys. Res.*, *107*, 5026.
- Figueredo P. H., Greeley R., Neuer S., Irwin L., and Schulze-Makuch D. (2003) Locating potential biosignatures on Europa from surface geology observations. *Astrobiology*, *3*, 851–861.
- Fischer H. J. and Spohn T. (1990) Thermal orbital histories of viscoelastic models of Io (J1). *Icarus*, *83*, 39–65.
- Freeman J., Moresi L., and May D. A. (2006) Thermal convection with a water ice I rheology: Implications for icy satellite evolution. *Icarus*, *180*, 251–264.
- Friedson A. J. and Stevenson D. J. (1983) Viscosity of rock-ice mixtures and applications to the evolution of icy satellites. *Icarus*, *56*, 1–14.
- Gaidos E. and Nimmo F. (2000) Tectonics and water of Europa. *Nature*, *405*, 637.
- Gammon P. H., Kieft H., Clouter M. J., and Denner W. W. (1983) Elastic constants of artificial and natural ice samples by Brillouin spectroscopy. *J. Glaciol.*, *29*, 433–459.
- Geissler P. E. and 14 colleagues (1998a) Evidence for non-synchronous rotation of Europa. *Nature*, *391*, 368–379.
- Geissler P. E. and 16 colleagues (1998b) Evolution of lineaments on Europa: Clues from Galileo multispectral imaging observations. *Icarus*, *135*, 107–126.
- Giese B., Oberst J., Roatsch T., Neukum G., Head J. W., and Pappalardo R. T. (1998) The local topography of Uruk Sulcus and Galileo Regio obtained from stereo data. *Icarus*, *135*, 303–316.

- Golombek M. P. and Banerdt W. B. (1986) Early thermal profiles and lithospheric strength of Ganymede from extensional tectonic features. *Icarus*, *68*, 252–265.
- Goldsby D. L. and Kohlstedt D. L. (2001) Superplastic deformation of ice: Experimental observations. *J. Geophys. Res.*, *106*, 11017–11030.
- Goodman J. C., Collins G. C., Marshall J., and Pierrehumbert R. T. (2004) Hydrothermal plume dynamics on Europa: Implications for chaos formation. *J. Geophys. Res.*, *109*, E03008.
- Grasset O. and Parmentier E. M. (1998) Thermal convection in a volumetrically heated, infinite Prandtl number fluid with a strongly temperature-dependent viscosity: Implications for planetary thermal evolution. *J. Geophys. Res.*, *103*, 18171–18181.
- Greeley R., Collins G. C., Spaun N. A., Sullivan R. J., Moore J. M., et al. (2000) Geologic mapping of Europa. *J. Geophys. Res.*, *105*, 22559–22578.
- Greeley R., Chyba C. F., Head J. W., McCord T. B., McKinnon W. B., Pappalardo R. T., and Figueredo P. (2004) Geology of Europa. In *Jupiter: The Planet, Satellites and Magnetospheres* (F. Bagenal et al., eds.), pp. 329–362. Cambridge Univ., Cambridge.
- Greenberg R. (2004) The evil twin of Agenor: Tectonic convergence on Europa. *Icarus*, *167*, 313–319.
- Greenberg R. and Geissler P. (2002) Europa's dynamic icy crust. *Meteoritics & Planet. Sci.*, *37*, 1685–1710.
- Greenberg R. and Weidenschilling S. J. (1984) How fast do Galilean satellites spin? *Icarus*, *58*, 186–196.
- Greenberg R. and 9 colleagues (1998) Tectonic processes on Europa: Tidal stresses, mechanical response and visible features. *Icarus*, *135*, 64–78.
- Greenberg R., Geissler P., Hoppa G., and Tufts B. R. (2002) Tidal tectonic processes and their implications for the character of Europa's icy crust. *Rev. Geophys.*, *40*, 1004.
- Greenberg R., Hoppa G. V., Bart G., and Hurford T. (2003) Tidal stress patterns on Europa's crust. *Cel. Mech. Dyn. Astron.*, *87*, 171–188.
- Gribb T. T. and Cooper R. F. (1998) Low-frequency shear attenuation in polycrystalline olivine: Grain boundary diffusion and the physical significance of the Andrade model for viscoelastic rheology. *J. Geophys. Res.*, *103*, 27627–27279.
- Han L. and Showman A. P. (2005) Thermo-compositional convection in Europa's icy shell with salinity. *Geophys. Res. Lett.*, *32*, L20201, DOI: 10.1029/2005GL023979.
- Han L. J. and Showman A. P. (2008) Implications of shear heating and fracture zones for ridge formation on Europa. *Geophys. Res. Lett.*, *35*, L03202.
- Hand K. P. and Chyba C. F. (2007) Empirical constraints on the salinity of the european ocean and implications for a thin ice shell. *Icarus*, *189*, 424–438.
- Harada Y. and Kurita K. (2007) Effect of non-synchronous rotation on surface stress upon Europa: Constraints on surface rheology. *Geophys. Res. Lett.*, *34*, L11204.
- Hawkes I. and Mellor M. (1972) Deformation and fracture of ice under uniaxial stress. *J. Glaciol.*, *11*, 103–131.
- Head J. W. and Pappalardo R. T. (1999) Brine mobilization during lithospheric heating on Europa: Implications for formation of chaos terrain, lenticula texture, and color variations. *J. Geophys. Res.*, *104*, 27143–27155.
- Head J. W., Pappalardo R. T., and Sullivan R. (1999) Europa: Morphological characteristics of ridges and triple bands from Galileo data (E4 and E6) and assessment of a linear diapirism model. *J. Geophys. Res.*, *104*, 18907–18924.
- Helfenstein P. and Parmentier E. M. (1985) Patterns of fracture and tidal stresses due to nonsynchronous rotation — implications for fracturing on Europa. *Icarus*, *61*, 175–184.
- Hoppa G. V., Tufts B. R., Greenberg R., and Geissler P. E. (1999a) Formation of cycloidal features on Europa. *Science*, *285*, 1899–1902.
- Hoppa G. V., Greenberg R., Geissler P., Tufts B. R., Plassmann J., and Durda D. D. (1999b) Rotation of Europa: Constraints from terminator and limb positions. *Icarus*, *137*, 341–347.
- Hoppa G., Tufts B. R., Greenberg R., and Geissler P. (1999c) Strike-slip faults on Europa: Global shear patterns driven by tidal stress. *Icarus*, *141*, 287–298.
- Hoppa G., Tufts B. R., Greenberg R., Hurford T. A., O'Brien D. P., and Geissler P. E. (2001) Europa's rate of rotation derived from the tectonic sequence in the Astypalaea region. *Icarus*, *153*, 208–213.
- Hurford T. A., Beyer R. A., Schmidt B., Preblich B., Sarid A. R., and Greenberg R. (2005) Flexure of Europa's lithosphere due to ridge-loading. *Icarus*, *177*, 80–396.
- Hurford T. A., Sarid A. R., and Greenberg R. (2007) Cycloidal cracks on Europa: Improved modeling and non-synchronous rotation implications. *Icarus*, *186*, 218–233.
- Hessinger J., White B. E., and Pohl R. O. (1996) Elastic properties of amorphous and crystalline ice films. *Planet. Space Sci.*, *44*, 937–944.
- Hussmann H. and Spohn T. (2004) Thermal-orbital evolution of Io and Europa. *Icarus*, *171*, 391–410.
- Hussmann H., Spohn T., and Wiczerkowski K. (2002) Thermal equilibrium states of Europa's ice shell: Implications for internal ocean thickness and surface heat flow. *Icarus*, *156*, 143–151.
- Jackson J. A. and White N. J. (1989) Normal faulting in the super continental crust: Observations from regions of active extension. *J. Struct. Geol.*, *11*, 15–36.
- Jankowski D. G. and Squyres S. W. (1991) Sources of error in planetary photogrammetry. *J. Geophys. Res.*, *96*, 20907–20922.
- Johnson R. E., Carlson R. S., Cooper J. F., Paranicas C., Moore M. H., and Wong M. C. (2004) Radiation effects on the surfaces of the Galilean satellites. In *Jupiter: The Planet, Satellites and Magnetospheres* (F. Bagenal et al., eds.), pp. 485–512. Cambridge Univ., Cambridge.
- Kargel J. S. (1998) Physical chemistry of ices in the outer solar system. In *Solar System Ices* (B. Schmidt et al., eds.), pp. 3–32. Kluwer, Dordrecht.
- Kattenhorn S. A. (2002) Nonsynchronous rotation evidence and fracture history in the Bright Plains region, Europa. *Icarus*, *157*, 490–506.
- Kattenhorn S. A. (2005) Strike-slip fault evolution on Europa: Evidence from tailcrack geometries. *Icarus*, *172*, 582–602.
- Kattenhorn S. A. and Marshall S. T. (2006) Fault-induced perturbed stress fields and associated tensile and compressive deformation at fault tips in the ice shell of Europa: Implications for fault mechanics. *J. Struct. Geol.*, *28*, 2204–2221.
- Kimura J., Yamagishi Y., and Kurita K. (2007) Tectonic history of Europa: Coupling between internal evolution and surface stresses. *Earth Planets Space*, *59*, 113–125.
- Kirk R. L., Barrett J. M., and Soderblom L. A. (2003) Photogrammetry made simple . . . ? In *Workshop on Advances in Planetary Mapping*, Houston, Texas. Available online at astrogeology.usgs.gov/Projects/ISPRS/MEETINGS/Houston2003/abstracts/Kirk\_isprs\_mar03.pdf.

- Kivelson M. G., Khurana K. K., Russell C. T., Volwerk M., Walker R. J., and Zimmer C. (2000) Galileo magnetometer measurements: A stronger case for a subsurface ocean at Europa. *Science*, 289, 1340–1343.
- Klinger J. (1980) Influence of a phase transition of ice on the heat and mass balance of comets. *Science*, 209, 271–272.
- Kovach D. L. and Chyba C. F. (2001) Seismic detectability of a subsurface ocean on Europa. *Icarus*, 150, 279–287.
- Lee S., Zanolin M., Thode A. M., Pappalardo R. T., and Makris N. C. (2003) Probing Europa's interior with natural sound waves. *Icarus*, 165, 144–167.
- Lee S., Pappalardo R. T., and Makris N. C. (2005) Mechanics of tidally driven fractures in Europa's ice shell. *Icarus*, 177, 367–379.
- Leith A. C. and McKinnon W. B. (1996) Is there evidence for polar wander on Europa? *Icarus*, 120, 387–398.
- Luttrell K. and Sandwell D. (2006) Strength of the lithosphere of the Galilean satellites. *Icarus*, 183, 159–167.
- Manga M. and Sinton A. (2004) Formation of bands, ridges and grooves on Europa by cyclic deformation: Insights from analogue wax experiments. *J. Geophys. Res.*, 109(E9), E09001, DOI: 10.1029/2004JE002249.
- Manga M. and Wang C. Y. (2007) Pressurized oceans and the eruption of liquid water on Europa and Enceladus. *Geophys. Res. Lett.*, 34, L07202, DOI: 10.1029/2007GL029297.
- Marshall S. T. and Kattenhorn S.A. (2005) A revised model for cycloid growth mechanics on Europa: Evidence from surface morphologies and geometries. *Icarus*, 177, 341–366.
- Matsuyama I. and Nimmo F. (2008) Tectonic patterns on reoriented and despun planetary bodies. *Icarus*, 195, 459–473.
- McCord T. B. and 12 colleagues (1998) Non-water-ice constituents in the surface material of the icy Galilean satellites from the Galileo near-infrared mapping spectrometer investigation. *J. Geophys. Res.*, 103, 8603–8626.
- McEwen A. S. (1986) Tidal reorientation and fracturing on Jupiter's moon Europa. *Nature*, 321, 49–51.
- McGovern P. J. and 9 colleagues (2002) Localized gravity/topography admittance and correlation spectra on Mars: Implications for regional and global evolution. *J. Geophys. Res.*, 107, 5136.
- McKinnon W. B. (1999) Convective instability in Europa's floating ice shell. *Geophys. Res. Lett.*, 26, 951–954.
- McKinnon W. B. (2006) On convection in ice I shells of outer solar system bodies, with detailed application to Callisto. *Icarus*, 183, 435–450.
- McNutt M. K. (1984) Lithospheric flexure and thermal anomalies. *J. Geophys. Res.*, 89, 1180–1194.
- Melosh H. J. (1989) *Impact Cratering: A Geologic Process*. Oxford, New York.
- Melosh H. J. (1980) Tectonic patterns on a tidally distorted planet. *Icarus*, 43, 334–337.
- Meyer J. and Wisdom J. (2007) Tidal heating in Enceladus. *Icarus*, 188, 535–539.
- Mitri G. and Showman A. P. (2005) Convective-conductive transitions and sensitivity of a convecting ice shell to perturbations in heat flux and tidal-heating rate: Implications for Europa. *Icarus*, 177, 447–460.
- Miyamoto H., Mitri G., Showman A. P., and Dohm J. M. (2005) Putative ice flows on Europa: Geometric patterns and relation to topography collectively constrain material properties and effusion rates. *Icarus*, 177, 413–424.
- Moore J. C. (2000) Models of radar absorption in European ice. *Icarus*, 147, 292–300.
- Moore J. M. and 25 colleagues (2001) Impact features on Europa: Results of the Galileo Europa Mission (GEM). *Icarus*, 151, 93–111.
- Moore W. B. (2006) Thermal equilibrium in Europa's ice shell. *Icarus*, 180, 141–146.
- Moore W. B. and Schubert G. (2000) The tidal response on Europa. *Icarus*, 147, 317–319.
- Murray C. D. and Dermott S. F. (1999) *Solar System Dynamics*. Cambridge Univ., Cambridge.
- Neukum G. (1997) Bombardment history of the jovian system. In *The Three Galileos: The Man, the Spacecraft, the Telescope* (C. Barbieri et al., eds.), pp. 201–212. Kluwer, Norwell, Massachusetts.
- Nimmo F. (2004a) Non-Newtonian topographic relaxation on Europa. *Icarus*, 168, 205–208.
- Nimmo F. (2004b) Stresses generated in cooling viscoelastic ice shells: Application to Europa. *J. Geophys. Res.*, 109, E12001.
- Nimmo F. (2004c) What is the Young's modulus of ice? In *Workshop on Europa's Icy Shell*, Abstract #7005. Lunar and Planetary Institute, Houston.
- Nimmo F. (2004d) Dynamics of rifting and modes of extension on icy satellites. *J. Geophys. Res.*, 109, E01003.
- Nimmo F. and Gaidos E. (2002) Thermal consequences of strike-slip motion on Europa. *J. Geophys. Res.*, 107, 5021, DOI: 10.1029/2000JE001476.
- Nimmo F. and Giese B. (2005) Thermal and topographic tests of Europa chaos formation models from Galileo E15 observations. *Icarus*, 177, 327–341.
- Nimmo F. and Manga M. (2002) Causes, characteristics and consequences of convective diapirism on Europa. *Geophys. Res. Lett.*, 29, DOI: 10.1029/2002GL015754.
- Nimmo F. and Matsuyama I. (2007) Reorientation of icy satellites by impact basins. *Geophys. Res. Lett.*, 34, L21201.
- Nimmo F. and Schenk P. (2006) Normal faulting on Europa: Implications for ice shell properties. *J. Struct. Geol.*, 28, 2194–2203.
- Nimmo F. and Pappalardo R. T. (2004) Furrow flexure and ancient heat flux on Ganymede. *Geophys. Res. Lett.*, 31, L19701.
- Nimmo F., Pappalardo R. T., and Giese B. (2003a) On the origins of band topography, Europa. *Icarus*, 166, 21–32.
- Nimmo F., Giese B., and Pappalardo R. T. (2003b) Estimates of Europa's ice shell thickness from elastically-supported topography. *Geophys. Res. Lett.*, 30, 1233, DOI: 10.1029/2002GL016660.
- Nimmo F., Thomas P. C., Pappalardo R. T., and Moore W. B. (2007a) The global shape of Europa: Constraints on lateral shell thickness variations. *Icarus*, 191, 183–192.
- Nimmo F., Spencer J. R., Pappalardo R. T., and Mullen M. E. (2007b) Shear heating as the origin of the plumes and heat flux on Enceladus. *Nature*, 447, 289–291.
- O'Brien D. P., Geissler P., and Greenberg R. (2002) A melt-through model for chaos formation on Europa. *Icarus*, 156, 152–161.
- Ojakangas G. W. and Stevenson D. J. (1986) Episodic volcanism of tidally heated satellites with application to Io. *Icarus*, 66, 341–358.
- Ojakangas G. W. and Stevenson D. J. (1989a) Thermal state of an ice shell on Europa. *Icarus*, 81, 220–241.
- Ojakangas G. W. and Stevenson D. J. (1989b) Polar wander of an

- ice shell on Europa. *Icarus*, 81, 242–270.
- Panning M., Lekic V., Manga M., Cammarano F., and Romanowicz B. (2006) Long-period seismology on Europa: 2. Predicted seismic response. *J. Geophys. Res.*, 111, E12008.
- Pappalardo R. T. and Barr A. C. (2004) The origin of domes on Europa: The role of thermally induced compositional diapirism. *Geophys. Res. Lett.*, 31, DOI: 10.1029/2003GL019202.
- Pappalardo R. T. and 10 colleagues (1998) Geological evidence for solid-state convection in Europa's ice shell. *Nature*, 391, 365–368.
- Pappalardo R. T. and 31 colleagues (1999) Does Europa have a subsurface ocean? Evaluation of the geological evidence. *J. Geophys. Res.*, 104, 24015–24055.
- Patterson G. W., Head J. W., and Pappalardo R. T. (2006) Plate motion on Europa and nonrigid behaviour of the icy lithosphere: The Castalia Macula region. *J. Struct. Geol.*, 28, 2237–2258.
- Phillips C. B., McEwen A. S., Hoppa G. V., Fagents S. A., Greeley R., Klemaszewski J. E., Pappalardo R. T., Klaasen K. P., and Breneman H. H. (2000) The search for current geologic activity on Europa. *J. Geophys. Res.*, 105, 22579–22598.
- Porco C. and 24 colleagues (2006) Cassini observes the active south pole of Enceladus. *Science*, 311, 1393–1401.
- Prockter L. M. and Pappalardo R. T. (2000) Folds on Europa: Implications for crustal cycling and accommodation of extension. *Science*, 289, 941–943.
- Prockter L. and Schenk P. (2005) Origin and evolution of Castalia Macula, an anomalous young depression on Europa. *Icarus*, 177, 305–326.
- Prockter L. M., Head J. W., Pappalardo R. T., Sullivan J. R., Clifton A. E., Giese B., Wagner R., and Neukum G. (2002) Morphology of European bands at high resolution: A mid-ocean ridge-type rift mechanism. *J. Geophys. Res.*, 107, DOI: 10.1029/2000JE001458.
- Qin R., Buck W. R., and Germanovich L. (2007) Comment on “Mechanics of tidally driven fractures in Europa's ice shell,” by S. Lee, R. T. Pappalardo, and N. C. Makris. *Icarus*, 189, 595–597.
- Riley J., Hoppa G. V., Greenberg R., Tufts B. R., and Geissler P. (2000) Distribution of chaotic terrain on Europa. *J. Geophys. Res.*, 105, 22599–22615.
- Rist M. A. (1997) High-stress ice fracture and friction. *J. Phys. Chem.*, 101, 6263–6266.
- Ross M. N. and Schubert G. (1987) Tidal heating in an internal ocean model of Europa. *Nature*, 325, 133–134.
- Ross M. N. and Schubert G. (1989) Viscoelastic models of tidal heating in Enceladus. *Icarus*, 78, 90–101.
- Ruiz J., Alvarez-Gomez J. A., Tejero R., and Sanchez N. (2007) Heat flow and thickness of a convective ice shell on Europa for grain size-dependent rheologies. *Icarus*, 190, 145–154.
- Sandwell D., Rosen P., Moore W., and Gurrola E. (2004) Radar interferometry for measuring tidal strains across cracks on Europa. *J. Geophys. Res.*, 109, E11003.
- Sarid A. R., Greenberg R., Hoppa G. V., Hurford T. A., Tufts B. R., and Geissler P. (2002) Polar wander and surface convergence of Europa's ice shell: Evidence from a survey of strike-slip displacement. *Icarus*, 158, 24–41.
- Sarid A. R., Greenberg R., Hoppa G. V., Geissler P., and Preblich B. (2004) Crack azimuths on Europa: Time sequence in the southern leading face. *Icarus*, 168, 144–157.
- Sarid A. R., Greenberg R., and Hurford T. A. (2006) Crack azimuths on Europa: Sequencing of the northern leading hemisphere. *J. Geophys. Res.*, 111, E08004.
- Schenk P. M. (2002) Thickness constraints on the icy shells of the Galilean satellites from a comparison of crater shapes. *Nature*, 417, 419–421.
- Schenk P. M. and Pappalardo R. T. (2004) Topographic variations in chaos on Europa: Implications for diapiric formation. *Geophys. Res. Lett.*, 31, L16703.
- Schenk P. M., Matsuyama I., and Nimmo F. (2008) True polar wander on Europa from global-scale small-circle depressions. *Nature*, 453, 368–371.
- Schilling N., Neubauer F. M., and Saur J. (2008) Time-varying interaction of Europa with the jovian magnetosphere: Constraints on the conductivity of Europa's subsurface ocean. *Icarus*, 192, 41–55.
- Schmeltz M., Rignot E., and Macayeal D. (2002) Tidal flexure along ice-sheet margins: Comparison of InSAR with an elastic-plate model. *Ann. Glaciol.*, 34, 202–208.
- Schulson E. M. (2002) On the origin of a wedge crack within the icy crust of Europa. *J. Geophys. Res.*, 107, 5107, DOI: 10.1029/2001JE001586.
- Schubert G., Anderson J. D., Spohn T., and McKinnon W. B. (2004) Interior composition, structure and dynamics of the Galilean satellites. In *Jupiter: The Planet, Satellites and Magnetospheres* (F. Bagenal et al., eds.), pp. 281–306. Cambridge Univ., Cambridge.
- Schwartz J. and Weeks W. F. (1977) Engineering properties of sea ice. *J. Glaciol.*, 19, 499–531.
- Showman A. P. and Han L. J. (2004) Numerical simulations of convection in Europa's ice shell: Implications for surface features. *J. Geophys. Res.*, 109, E01010.
- Showman A. P. and Han L. J. (2005) Effects of plasticity on convection in an ice shell: Implications for Europa. *Icarus*, 177, 425–437.
- Showman A. P., Mosqueira I., and Head J. W. (2004) On the resurfacing of Ganymede by liquid-water volcanism. *Icarus*, 172, 625–640.
- Solomatov V. S. (1995) Scaling of temperature- and stress-dependent viscosity convection. *Phys. Fluids*, 7, 266–274.
- Sotin C., Head J. W., and Tobie G. (2002) Europa: Tidal heating of upwelling thermal plumes and the origin of lenticulae and chaos melting. *Geophys. Res. Lett.*, 29, DOI: 10.1029/2001GL013844.
- Spaun N. A. and Head J. W. (2001) A model of Europa's crustal structure: Recent Galileo results and implications for an ocean. *J. Geophys. Res.*, 106, 7567–7575.
- Spaun N. A., Head J. W., Collins G. C., Prockter L. M., and Pappalardo R. T. (1998) Conamara Chaos region, Europa: Reconstruction of mobile polygonal ice blocks. *Geophys. Res. Lett.*, 25, 4277–4280.
- Spencer J. R., Tamppari L. K., Martin T. A., and Travis L. D. (1999) Temperatures on Europa from Galileo photopolarimeter-radiometer: Nighttime thermal anomalies. *Science*, 284, 1514–1516.
- Spencer J. R., Pearl J. C., Segura M., Flasar F. M., Mamoutkine A., Romani P., Buratti B. J., Hendrix A. R., Spilker L. J., and Lopes R. M. C. (2006) Cassini encounters Enceladus: Background and the discovery of a south polar hot spot. *Science*, 311, 1401–1405.
- Spohn T. and Schubert G. (2003) Oceans in the icy Galilean satellites of Jupiter? *Icarus*, 161, 456–467.

- Squyres S. W., Reynolds R. T., Cassen P. M., and Peale S. J. (1983) Liquid water and active resurfacing on Europa. *Nature*, *301*, 225–226.
- Stempel M. M., Barr A. C., and Pappalardo R. T. (2005) Model constraints on the opening rates of bands on Europa. *Icarus*, *177*, 297–304.
- Stevenson D. J. (2000) Limits on the variation of thickness of Europa's ice shell (abstract). In *Lunar and Planetary Science XXXI*, Abstract #1506. Lunar and Planetary Institute, Houston (CD-ROM).
- Strom R. G., Schaber G. G., and Dawson D. D. (1994) The global resurfacing of Venus. *J. Geophys. Res.*, *99*, 10899–10926.
- Sullivan R. and 11 colleagues (1998) Episodic plate separation and fracture infill on the surface of Europa. *Nature*, *391*, 371–373.
- Thomson R. E. and Delaney J. R. (2001) Evidence for a weakly stratified euroman ocean sustained by seafloor heat flux. *J. Geophys. Res.*, *106*, 12355–12365.
- Tobie G., Choblet G., and Sotin C. (2003) Tidally heat convection: Constraints on Europa's ice shell thickness. *J. Geophys. Res.*, *108*, 5124, DOI: 10.1029/2003JE002099.
- Tobie G., Mocquet A., and Sotin C. (2005) Tidal dissipation within large icy satellites: Applications to Europa and Titan. *Icarus*, *177*, 534–549.
- Turcotte D. L. and Schubert G. (2002) *Geodynamics*. Cambridge Univ., Cambridge. 456 pp.
- Turtle E. P. and Ivanov B. A. (2002) Numerical simulations of impact crater excavation and collapse on Europa: Implications for ice thickness (abstract). In *Lunar and Planetary Science XXXIII*, Abstract #1431. Lunar and Planetary Institute, Houston (CD-ROM).
- Turtle E. P. and Pierazzo E. (2001) Thickness of a euroman ice shell from impact crater simulations. *Science*, *294*, 1326–1328.
- Van Hoolst T., Rambaux N., Karatekin O., Dehant V., and Rivoldini A. (2008) The librations, shape and icy shell of Europa. *Icarus*, *195*, 386–399.
- Vaughan D. G. (1995) Tidal flexure at ice shelf margins. *J. Geophys. Res.*, *100*, 6213–6224.
- Wahr J., Zuber M. T., Smith D. E., and Lunine J. I. (2006) Tides on Europa, and the thickness of europa's icy shell. *J. Geophys. Res.*, *111*, E12005, DOI: 10.1029/2006JE002729.
- Wahr J., Selvans Z. A., Mullen M. E., Barr A. C., Collins G. C., Selvans M. M., and Pappalardo R. T. (2008) Modelling stresses on satellites due to non-synchronous rotation and orbital eccentricity using gravitational potential theory. *Icarus*, in press.
- Watts A. B. (2001) *Isostasy and Flexure of the Lithosphere*. Cambridge Univ., Cambridge.
- Williams K. K. and Greeley R. (1998) Estimates of ice thickness in the Conamara Chaos region of Europa. *Geophys. Res. Lett.*, *25*, 4273–4276.
- Wilson L., Head J. W., and Pappalardo R. T. (1997) Eruption of lava flows on Europa: Theory and application to Thrace Macula. *J. Geophys. Res.*, *102*, 9263–9272.
- Yoder C. F. (1979) How tidal heating in Io drives the Galilean orbital resonance locks. *Nature*, *279*, 767–770.
- Zahnle K., Schenk P., Sobieszczyk S., Dones L., and Levison H. F. (2001) Differential cratering of synchronously rotating satellites by ecliptic comets. *Icarus*, *153*, 111–129.
- Zahnle K., Schenk P., Levison H., and Dones L. (2003) Cratering rates in the outer solar system. *Icarus*, *163*, 263–289.
- Zimmer C., Khurana K. K., and Kivelson M. G. (2000) Subsurface oceans on Europa and Callisto: Constraints from Galileo magnetometer observations. *Icarus*, *147*, 329–347.